CHEMISTRY
A EUROPEAN JOURNAL

DOI: 10.1002/chem.200903335

Preparation and Characterisation of Super-Hydrophobic Surfaces

Colin R. Crick and Ivan P. Parkin*[a]

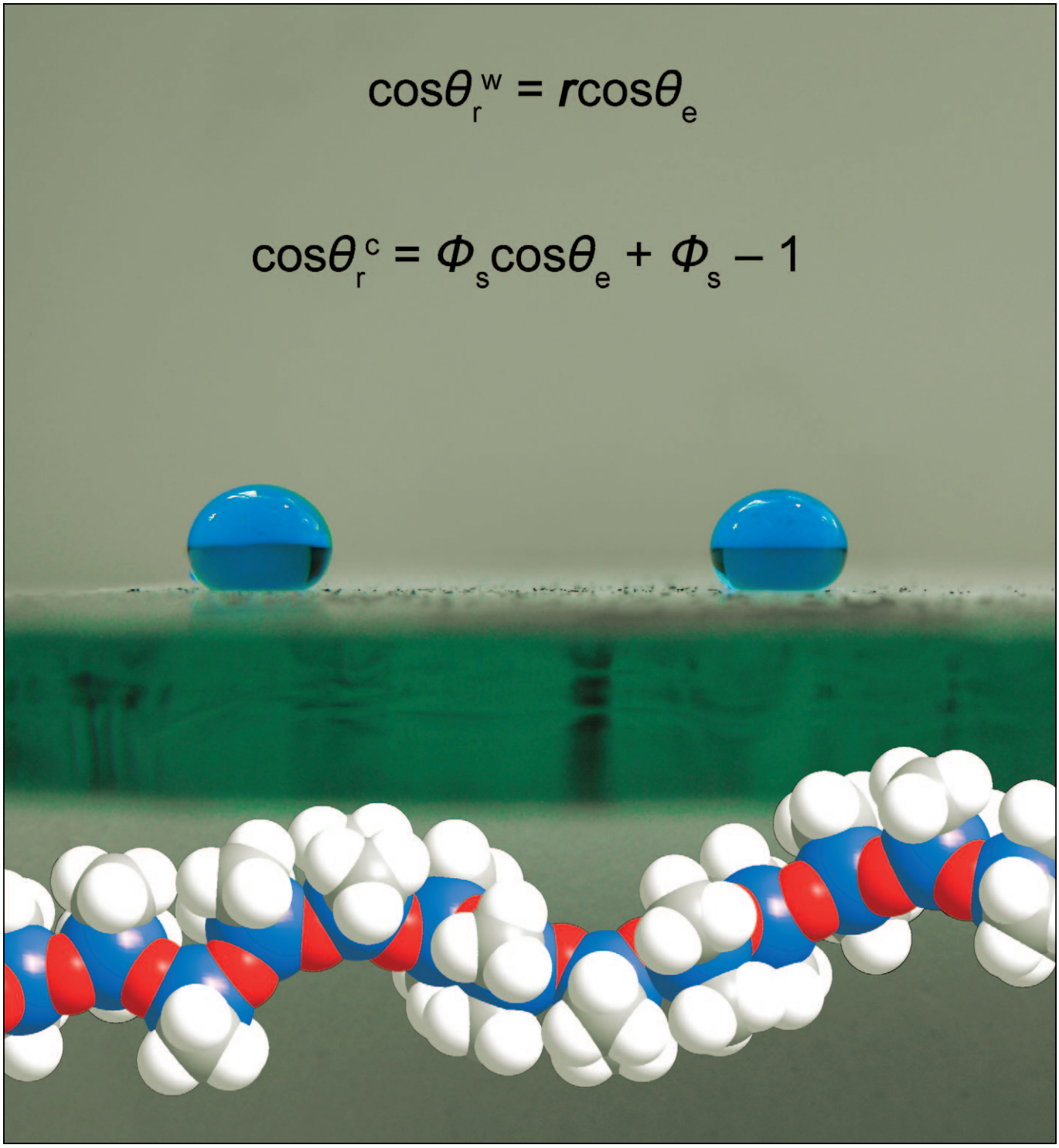

Abstract: The interest in highly water-repellent surfaces has grown in recent years due to the desire for self-cleaning surfaces. A super-hydrophobic surface is one that achieves a water contact angle of 150° or greater. This article explores the different approaches used to construct super-hydrophobic surfaces and identifies the key properties of each surface that contribute to its hydrophobicity. The models used to describe surface interaction with water are considered, with attention directed to the methods of contact angle analysis. A summary describing the different routes to hydrophobicity is also given.

Keywords: hydrophobic effect · lotus effect · self-cleaning · super-hydrophobicity · surface chemistry · water-repellent materials

Introduction

The purpose of this review is to detail and classify the methods used to make surfaces that are super-hydrophobic to water droplets. We start with an overview of the ways in which nature generates hydrophobic surfaces through the "lotus effect". The second section details the underlying theory used to describe the interaction of water droplets with super-hydrophobic surfaces through the Cassie–Baxter and Wenzel models, in which the water either sits on the surface protrusions or manages to penetrate the surface porosity, respectively; this section presents the different methods used to calculate water contact angles, and provides a note of caution on comparing one study with another because a plethora of different techniques are used to measure the same quantity. The third section details the main synthetic routes used to make super-hydrophobic surfaces, and the fourth section summarises these routes and classify them by type and concludes with some of the applications for super-hydrophobic surfaces.

The current examinations of the literature in previously reported reviews cover extensive ranges of material.[1–4] This review aims to describe the most recent work carried out in the design and manufacture of super-hydrophobic surfaces. The main focus will be on the methods used to form these surfaces, in an attempt to encompass many techniques. Formulation of mechanisms to form super-hydrophobic surfaces has also been carried out by considering the different approaches to constructing hydrophobic surface. Additionally, the methods used to analyse hydrophobicity of surfaces by way of contact angle measurements will be examined. A detailed examination of the inconsistencies in measuring super-hydrophobic contact angles is presented.

The lotus effect: Water droplets can interact with a surface in a variety of ways. The nature of the interaction is related to how well water bonds to the surface compared with how well it bonds to itself. It ranges from super-hydrophilic,[5] in which the water can fully and effectively wet a surface to form a flat puddle due to a strong water–surface interaction, through to super-hydrophobic, in which water is effectively repelled from the surface to form a near-spherical droplet[6] and in which there is a weak water–surface interaction.

Super-hydrophobic surfaces are observed in nature, for example, in the lotus effect (named after the lotus plant, *Nelumbo nucifera*), which describes the self-cleaning action of some leaf surfaces. If the leaf shows high enough hydrophobicity, water will form near-spherical droplets that roll across the surface instead of sliding (Figure 1). The rolling

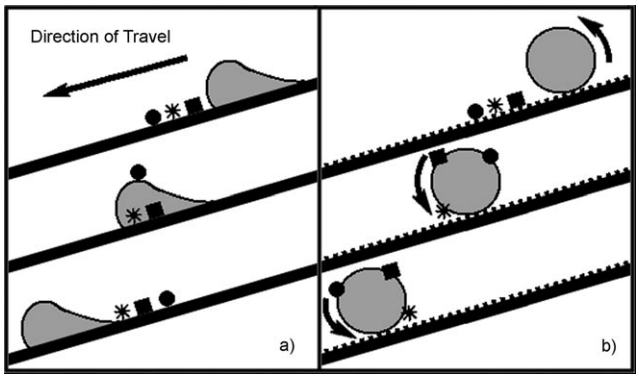

Figure 1. Diagram demonstrating the cleaning mechanism on smooth (a) and rough (b) super-hydrophobic surfaces.

action increases the amount of foreign bodies picked up.[7] Rougher surfaces tend to have the greatest self-cleaning action. The lotus leaf surface adopts this self-cleaning mechanism and facilitates the rolling of water droplets that collect dirt particles as they move.[8] The leaves themselves have a waxy surface coating that acts to repel water and also have protrusions that make the waxy surface highly rough (Figure 2). Both of these surface features combine to allow water droplets to roll and not slide.[9] The rough, nanoscale, hair-like structures (Figure 2) can also act to trap air underneath the water droplets, facilitating the rolling motion.[3] Leaves that are waxy but do not have the rough microstructure observed in the lotus plant are less efficient

[a] C. R. Crick, Prof. I. P. Parkin
Department of Chemistry
University College London
20 Gordon Street
London, WC1H 0AJ (UK)
Fax: (+44) 020-7679-7463
E-mail: i.p.parkin@ucl.ac.uk

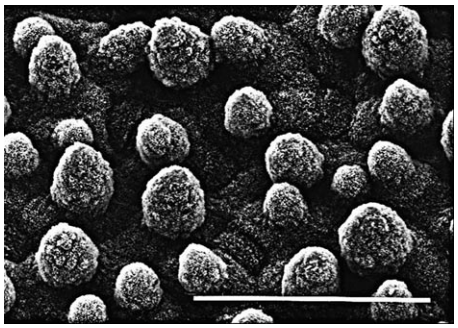

Figure 2. SEM images of *Nelumbo nucifera* (lotus) showing a highly rough surface microstructure (scale bar = 50 μm). Reproduced with permission from ref. [10].

at self-cleaning.[5] Plants that possess both a waxy and highly rough surface have far superior self-cleaning properties than those with comparable smooth waxy surfaces.[5]

Other examples of extreme hydrophobicity in nature include water strider legs (Figure 3), which have a highly defined microstructure that is coated by a layer of secreted wax.[11] The wings of some insects also show hydrophobic properties brought about by surface microstructure and composition.[12] Butterfly wings demonstrate super-hydrophobic properties, employing a directional rolling of water away from the body of the butterfly that is brought about by a network of microstructured scales on the wings surface.[13] It is these surface characteristics that have proven inspirational in the design of artificial hydrophobic surface. One nature-inspired method is to use a natural leaf surface for the imprint of polymer surfaces to render them hydrophobic.[14] The lotus leaf and other surfaces that exhibit the lotus effect demonstrate a hierarchical micro- and nanoscale roughness.

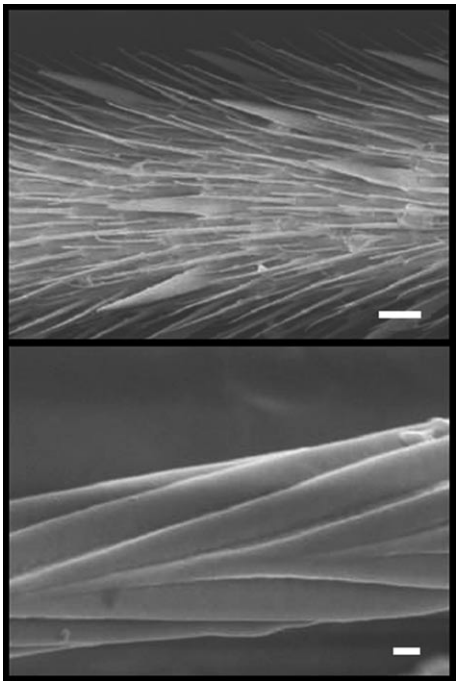

Figure 3. SEM images of a water strider leg. The spindle-like structures emanating off the leg (upper; scale bar = 20 μm) have a nanogroove structure (lower; scale bar = 200 nm) to further increase the roughness of the leg. This roughness combined with a secreted wax provides an extremely hydrophobic surface. Reproduced with permission from ref. [11].

Surface Models and Characterisation

Surface models: Models can be used to help predict and explain the way surface interacts with water. The two most commonly employed are the Wenzel[15] and the Cassie–Baxter models.[16] Both of these models use the water contact angle (θ), that is, the angle subtended by the droplet and the surface (Figure 4), as a direct measurement of surface hydrophobicity. If a surface has a contact angle with water that is greater than 90°, then the surface is classed as hydrophobic, if the contact angle is less than 90°, the surface is hydrophilic. The higher the contact angle, the more hydrophobic, or water-repellent, a surface is. The maximum contact angle is 180° for a completely spherical droplet. If the contact angle is reduced to less than 90°, then the surface is more hydrophilic, and it approaches 0° if the water sheets over the whole surface (i.e., super-hydrophilic coating).[17]

Surface (specific) energy: This is the measurement of how a water droplet will interact with a surface. If a droplet is in

Ivan Parkin is a Professor of Inorganic and Materials Chemistry at University College London. He obtained his first degree and Ph.D. at Imperial College and was a postdoctoral fellow at the University of Indiana. He was promoted to Professor at UCL in 2000. His laboratory focuses on the preparation of inorganic materials by innovative routes, and his group have developed new hydrophilic coatings on glass and new solid-state gas sensors by chemical vapour deposition.

Colin Crick is a Ph.D. student in Professor Parkin's laboratory. He studied chemistry at UCL from 2004 to 2008 and obtained a first class honours degree there. His research area is the chemical vapour deposition of thin films, with a focus on the design and preparation of hydrophobic surfaces.

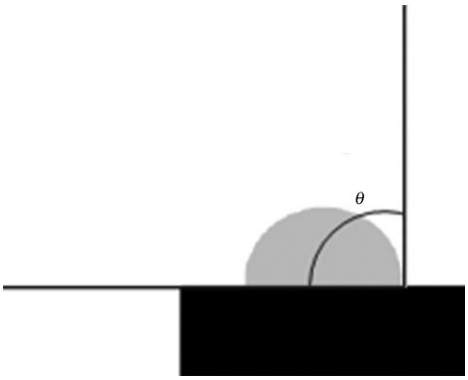

Figure 4. The water contact angle (θ) shown as the angle between the plane of a surface and the tangent at which the liquid droplet makes contact with the surface.

equilibrium, that is, if the contact angle is invariant, then the surface energy inside and outside the droplet are the same. If the energy of the surface inside a droplet is lower than that of the outside, the droplet will be liable to expand.[15] If the specific energy of a surface is relatively low, water will not be attracted as strongly, thus the contact angle will tend to be greater. Therefore, a surface with a lower surface energy will tend to be hydrophobic.

Surface roughness: The roughness of a surface can be defined by looking at the difference between the actual surface area, including peaks and valleys of surface morphology, and the planar or geometric area. The latter is the area of contact the water droplet makes with the surface assuming a totally smooth surface, whereas the actual surface area takes into account the protrusions. Both of these surfaces are used to calculate the roughness factor:

$$r = \text{roughness factor} = \frac{\text{actual surface area}}{\text{planar area}}$$

The roughness factor is incorporated directly into the Wenzel model,[15] whereas the Cassie–Baxter model uses a comparable measurement (see below). The two models can be compared because they have many similar features and they deal with the same type of interactions; however, there are some fundamental differences.[15]

The Cassie–Baxter model uses both advancing (θ_A) and receding (θ_R) contact angles. They can be measured in experiments that use tilted surfaces (Figure 5a). The receding contact angle can also be measured by dropping a water droplet onto a horizontal surface, then removing some of the water from the droplet and noting the contact angle when the area of contact begins to decrease (Figure 5b). Advancing contact angles can also be measured by adding volume to the water droplet and noting when the area of contact starts to increase (Figure 5c).[3]

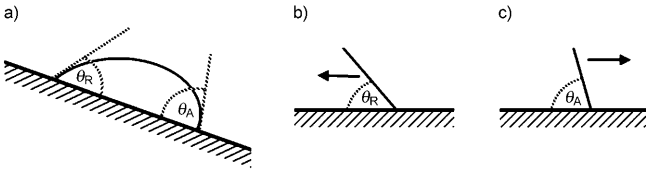

Figure 5. a) Determination of contact angles by tilting the surface until there is no further change in angle without movement of the droplet. b) Receding contact angle. c) Advancing contact angle.

Wenzel model:[15] The major premise of this model is that the water makes full contact with the surface, with no air trapped under the droplet. This model uses the surface tension of the solid and the water–solid interfacial tension. The roughness of the surface is considered by using the roughness factor (r) as described above, such that if a surface in constant surface tension has its roughness factor doubled, the energy of the surface per unit geometric structure will double. The Wenzel model uses force vectors to represent the change in surface properties when r is incorporated (Figure 6). The force vectors are represented by S_1 and S_{12}

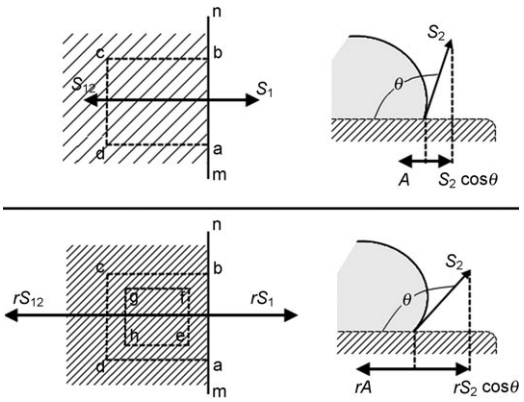

Figure 6. Diagram showing forces involved in the Wenzel model; S_1, S_2 and S_{12} represent the force vectors included in the adhesion tensions. The specific energy of the interface is represented by area a,b,c,d. Upon roughening, the area representing the specific energy of the surface is condensed to e,f,g,h. Reproduced with permission from ref. [15].

and their difference is the adhesion tension A, such that $A = S_1 - S_{12}$. The surface tension of the liquid (S_2), the contact angle (θ) and the adhesion tension (A) can be related by $A = S_2\cos\theta$, as shown in Figure 6. Combining these two equations gives $A = S_1 - S_{12} = S_2\cos\theta$ and applying surface roughness gives $rA = r(S_1 - S_{12}) = S_2\cos\theta$.

Cassie–Baxter (CB) model:[16,18] This model was devised after the Wenzel model was developed. It considers that the water droplet sits atop the protrusions of a surface and air is trapped underneath the droplet between these protrusions. This model can be related back to the Wenzel model. The Cassie–Baxter model considers the interaction with the surface in terms of interface areas and interfacial energies; f_1 is the solid–liquid interface area, f_2 is the liquid–air interface

area beneath the droplet and energies are represented as γ, in which γ_{LS} is the solid–liquid interfacial energy, γ_{SA} is the solid–air interfacial energy and γ_{LA} is the liquid–air interfacial energy. Thus, the products of the area and the energies will give the energy for that area. The net energy, E_D, of the model is expressed as:

$$E_D = f_1(\gamma_{LS} - \gamma_{SA}) + f_2\gamma_{LA}$$

Introducing the contact angle then gives:

$$\cos\theta_D = -\frac{E_D}{\gamma_{LA}} = f_1\cos\theta_A - f_2$$

in which θ_D is the apparent contact angle and θ_A is the advancing contact angle for the solid–liquid interface. In the same way, the equation for the receding contact angle can be derived,[19] which reduces to Wenzel's model in which $f_2 = 0$ (Figure 7).

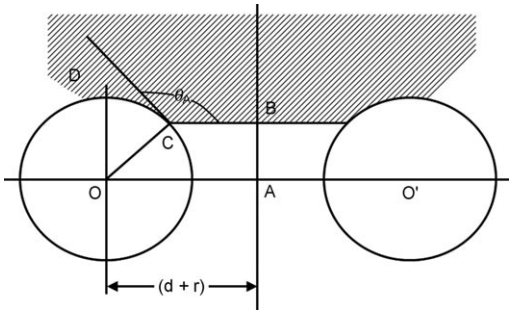

Figure 7. Diagram of the cross-section of two fibres, the length on the surfaces can be taken as OA, the positions on the cross-section (O,A,B,C,D) can be used to calculate the interfacial energies (f_1 and f_2).[12] The Cassie–Baxter model differs from the Wenzel model in that air is trapped underneath the water droplet between the surface protrusions. Reproduced with permission from ref. [16].

Both models can be successful in their aim of describing the interaction between water and a surface and neither can be shown to be superior. The relative success of each model depends on the nature of wetting observed on the surface being considered.[20] The key equation for each theory is shown in Figure 8; this demonstrates that both equations become the same when looking at flat surfaces (in which $r = \Phi_s = 1$).

The movement of water across a surface is also affected by the wetting nature of the surface. A Wenzel-type wetting mechanism means that there is complete contact between the surface and water droplet at any point of coverage (Figure 8), with no air trapped underneath. Because there is a greater area of contact between the water and the surface in the Wenzel model, movement across the surface is made harder.[3] For a Cassie–Baxter surface, not only is the water droplet-to-surface contact lower, but there is air trapped underneath, which makes the surface "slippery" (with respect to water). A Wenzel-type surface will be "sticky", with a lower likelihood of water droplets rolling across the surface; lotus-type self-cleaning is less likely to be observed. However, water droplets can move easily across a slippery Cassie–Baxter-type surface and a rolling action is more likely to be observed; it is this type of surface that is required for lotus-effect self-cleaning.

Intermediate states: The Wenzel model is aimed at surfaces at which the water droplet makes contact with all parts of the surface (Figure 8), whereas Cassie–Baxter uses a fraction of contact between the droplet and the surface, with flat points of contact. However, a pure form of either model may not be the case for some surfaces, that is, those that have no flat area of contact with the water droplet (Figure 9). If both the Wenzel and Cassie–Baxter models are combined, both the roughness factor (r) and the fraction of solid–liquid contact area can be used in an equation to describe such surfaces (Figure 9).[22]

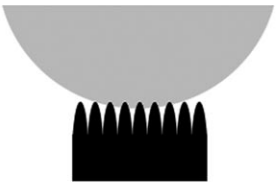

$$\cos\theta_r^{cw} = \Phi_s r\cos\theta_e + \Phi_s - 1$$

Figure 9. Diagram showing a Cassie–Baxter/Wenzel intermediate state with the key equation, in which θ_r^{cw} is the apparent contact angle, θ_e is the equilibrium contact angle on the flat surface and Φ_s is the area fraction of solid–liquid contact. The protrusions of the surface only partially penetrate the water droplet. The equation combines both of the surface model approaches. Reproduced with permission from ref. [22].

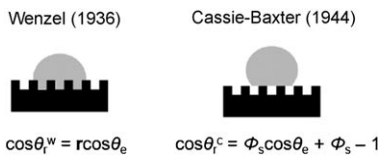

Figure 8. Diagram of the Cassie–Baxter and Wenzel approaches with their key equations, in which $\theta_r^{c/w}$ is the apparent contact angle upon assuming each theory, θ_e is the equilibrium contact angle on the flat surface and Φ_s is the area fraction of solid–liquid contact. Reproduced with permission from ref. [21].

The transition between the two wetting states is the subject of much study, with small changes in surface feature dimensions, such as protrusion height, size and separation, providing a large difference not only in the stickiness of a surface but also in the contact angle.[23,24] The air trapped under the water drops in the Cassie–Baxter mechanism acts to render the surface slippery and increase the contact angle further.[12] This air remains under the droplets because the water cannot penetrate the surface porosity to remove it, either because the water is greatly repelled by the low-

energy material of the surface and/or because the air cannot flow through the surface microstructure if displaced (i.e., the surface microstructure is not sinusoidal), so air is trapped under the water droplets in the latter case. The introduction of particular shapes in the surface microstructure of hydrophilic substrates (i.e., $\theta < 90°$ with flat surface) can result in a hydrophobic surface. This occurs because air trapped under the droplet, which would not be there if the surface was sinusoidal, acts to improve the resultant hydrophobicity.[25] Designing surfaces with these factors in mind can produce interesting surfaces; by giving a surface directional roughness (e.g., stripes across a surface), it can be imagined that a droplet rolling along (parallel to) the stripes will roll differently compared with a droplet rolling perpendicular to the stripes. This surface property has been demonstrated by using hexane droplets on a textured surface on which a large difference in contact angle occurs depending on the orientation of measurement.[26]

The evaporation of water on a surface can give an indication of the type of wetting mechanism that occurs.[27] Surfaces that are wetted in a Wenzel fashion are sticky in nature, so when the droplet reduces in volume through evaporation the area of contact remains the same but the contact angle is reduced. On slippery Cassie–Baxter surfaces, the area of contact decreases as the droplet reduces in volume and in consequence the contact angle remains unchanged until a very low droplet volume is reached. The transition from Cassie–Baxter wetting to Wenzel wetting can be achieve by addition of agents to the surface.[28]

Super-hydrophobicity: A super-hydrophobic surface is one that repels water to such an extent that the contact angles obtained are extremely high; they are generally defined as surfaces with water contact angles above 150°,[29] but it has also been less commonly adopted as 140°.[30] To form a surface with super-hydrophobic properties, a low-energy surface must be combined with high surface roughness. The highest known water contact angle on a smooth low-energy surface is around 110 to 120° (Table 1). Alkyl and fluorinated alkyl groups (as well as others[19,31]) typically have a low energy of interaction with water and have been used as super-hydrophobic surfaces because water is very strongly repelled by the surface, which results in an increase in contact angle.[32] Table 1 shows the relative hydrophobicities of such surfaces for purely flat surfaces with no surface microstructure; if surface roughness is introduced these composition types exhibit super-hydrophobic properties. The tilt angle of such a surface is typically less than 10° and is very likely to demonstrate the lotus self-cleaning effect.[33]

Table 1. Contact angles (θ) with water for planar surfaces composed of a pure array with CF_3, CF_2, CH_3 and CH_2 as terminal groups.[32]

Surface terminal group	θ [°]
CF_3	120
CF_2	108
CH_3	111
CH_2	94

The water contact angle is the most frequently used observation to measure the hydrophobicity of a surface. However, it is known that, due to gravitational forces on the water droplet, the contact angle will differ as the volume is changed,[1] with the water bowing with increased volume.[34] The method of analysis also strongly determines the resulting measured contact angle. In one case, analysis of an image showing the same 5 μL droplet (Figure 10) gave contact angles that varied from 152° to over 179°.[24] Therefore, it can be said that only droplets measured by using the same analysis system and the same droplet volume can be directly compared, but if either droplet volume and/or analysis techniques varies then a direct comparison cannot easily be made, although in practice this varies by less than 20°. These factors must be taken into account when comparing results from a range of sources because a difference in contact angle may not be solely due to differences in surface hydrophobicity, but may be also due to the methods used to collect the results. Many articles state which apparatus was used to measure the contact angles on a surface but fewer state the computational method used to analyse the droplets. Another issue that can also influence the observed success of a hydrophobic surface is the stating of average[35] or maximum contact angle values. The water contact angle values stated in this review do suffer from the inconsistencies mentioned above, so these issues must be considered when any comparison is done.

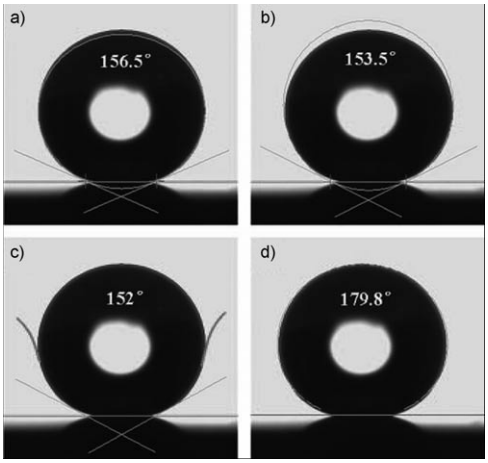

Figure 10. Images of a 5 μL water droplet on a super-hydrophobic surface. All images show the same droplet with the contact angle analysed by using a) ellipse fitting; b) circle fitting; c) tangent searching and d) Laplace–Young Fitting. These show that the same water droplet can give a range of results depending on the method of analysis. The lines shown are either horizontal baselines or shape simulation lines used in the calculation of the contact angle. Reproduced with permission from ref. [1].

Methods for Hydrophobic Surface Fabrication

This section reviews the various different methods used to synthesise hydrophobic and super-hydrophobic surfaces. The key factors responsible for changes in water contact angle are rationalised.

Fluoroalkylsilane (FAS) coatings: FAS molecules can interact with water in two ways, that is, in a hydrophobic/non-wetting or a hydrophilic/wetting manner depending on which end of the molecule is considered. In the examples below, the hydrophobic end is often CF_3-terminated. Figure 11 shows an example of a commercially available

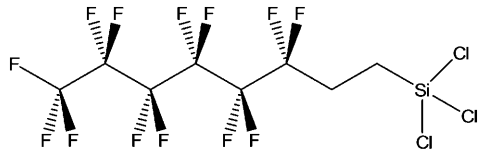

trichloro(tridecafluorooctyl)silane

Figure 11. An example of a fluoroalkylsilane (FAS) molecule. The fluorinated part of the molecule is shielded from any attractive interactions with water (hydrophobic). The silicon end possesses polarised bonds (Si–Cl in this example) that, if left exposed, can interact with water in a hydrophilic manner.

FAS molecule; the trichlorosilane part of the molecule is hydrophilic whereas the chain is hydrophobic. The trichloro-(tridecafluorooctyl)silane molecule cannot be directly used for formation of a hydrophobic surface because it has both hydrophobic and hydrophilic properties. However, modifying this type of molecule by means of polymerisation and hydration[36] can allow the hydrophilic part of the molecule to become reactive to a species on a surface. An example of this is shown in Figure 12; the polymerised silicon possesses a hydroxyl group that binds to a surface hydroxyl in a dehydration reaction. The result is that the hydrophobic fluorinated chain is left exposed on the surface and thus it repels water.

A study carried out by J. Bico et al.[38] used a silicon wafer surface as a substrate for the application of FAS. The FAS ($F(CF_2)_{10}(CH_2)_2SiCl_3$) was applied and grafted at 1100 °C for 2 h. The results clearly show that a flat surface with an applied FAS coating can be roughened to greatly change the contact angle, which increases from less than 118° on the flat surface to 167° on the spiked surface. The surfaces were created by moulding; an image of a created structure is given in Figure 13.[37]

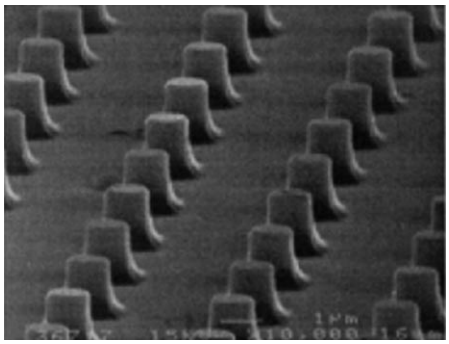

Figure 13. SEM image of a spiked hydrophobic surface designed to maximise the attainable contact angle. This structure allows for less water–surface contact when using the Cassie–Baxter model and gives both predicted and measured contact angles of 167°. Reproduced with permission from ref. [38].

A similar surface can be constructed by using a similar technique and following the same construction steps. Hydrolysis of the FAS followed by dehydration leads to polymerisation and thus binding of the modified species, which allows the hydrophobic part of the molecule to be exposed. The addition of an acrylic polymer to the reaction mixture results in a change in the microstructure and increases surface roughness as shown in Figure 14. Water contact angles of up to 152° were achieved on this surface.[39] The use of FAS molecules to coat surfaces has also been carried out by grafting onto already roughened substrates.[40]

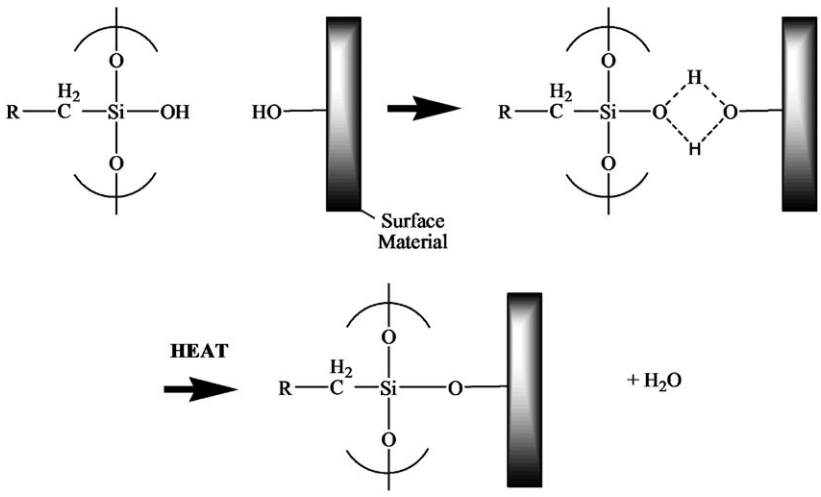

Figure 12. Proposed condensation reaction at a surface (hydroxyl groups) by using an altered FAS; R = hydrophobic chain of the FAS molecule.[37]

Poly(tetrafluoroethalene) (PTFE) surfaces: The chemical composition of PTFE provides an extremely low surface energy (Figure 15).[41] PTFE has a high molecular weight; it is a solid at room temperature and can, therefore, be shaped quite easily; roughening can be effec-

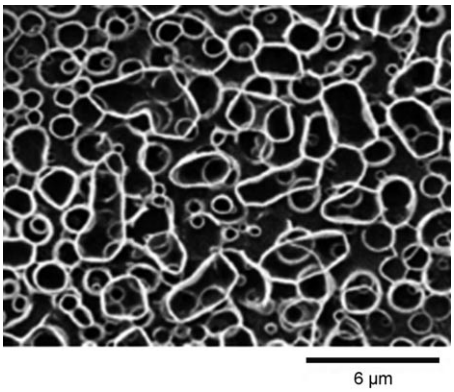

Figure 14. An SEM image of the acrylic polymer microstructure constructed by Nakajima et al.[28] to maximise the surface roughness and achieve a large contact angle.

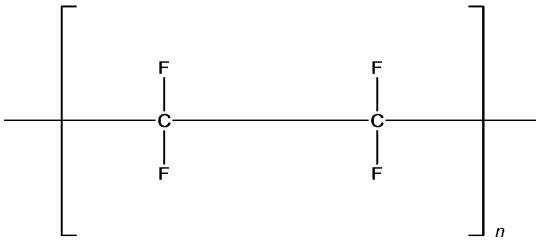

Figure 15. Basic representation of the structure of the PTFE molecule. This long-chain molecule is very hydrophobic and does not interact with water because there is little access to the polarised C–F bonds.

tive in increasing the hydrophobicity of this surface. Although there are many strategies imaginable for the modification of PTFEs, the basic principles remain the same: to allow the formation of a highly rough surface while maintaining the hydrophobicity of the composite materials.[42]

Plasma treatment of surfaces has been employed on flat PTFE surfaces.[41] Oxygen plasma was used to treat the flat PTFE, resulting in an increase in water contact angle from 118° to 131°. Addition of a fluorinated molecule (1*H*,1*H*,2*H*,2*H*-heptadecafluorodecyl acrylate) into the plasma resulted in a further increase to 148°. The action of the oxygen plasma was shown to have a roughening effect on the flat substrate, which was confirmed by atomic force microscopy (AFM). However, it also caused the introduction of foreign particles (i.e., not PTFE). When combined with a fluorinated acrylate in the plasma it allowed the foreign particles to be coated with fluorinated material, which enabled a further increase in the hydrophobicity.[41] Recent developments in the plasma treatment of PTFE surface has resulted in controllable roughening of surfaces and increased contact angles to super-hydrophobic magnitudes (≈162°).[43] The use of plasma as a surface-roughening method can be extended to other polymers, such as poly(L-lactic acid), in which controllable hydrophobicity across a substrate can be achieved.[44]

Additionally, silica microspheres have been used as a mould for a PTFE surface (Figure 16). The experiment involved sintering beads of various diameters onto a flat substrate and filling in the gaps with PTFE. Sintering a silica template of microspheres (diameter 850 nm) at 970 °C resulted in a rough PTFE surface with water contact angles of 154° after removal of the silica.[45]

The introduction of surface roughness via the spray-coating of suspensions has been achieved by using furfural acetone resin/PTFE mixtures. The droplets in the spray allow the gathering of PTFE material and agglomerations of particles on the surface (water contact angle 157°).[46] A slight variation on this spray-coating example uses a mixture of cellulose nitrate and fluoroacrylic polymer to bring about similar super-hydrophobic results, with a water contact angle of 165°.[47] Other methods include the addition of components to molten PTFE to induce surface roughness.[48]

Alkyl–ketene dimers (AKDs): The chemical structure of an AKD does not make it an obvious candidate for a super-hydrophobic surface, in that it has no alkyl or fluoroalkyl chains (Figure 17). It is a wax that, upon solidification from its melt, spontaneously forms a surface fractal pattern. This surface is highly rough, and it is this extreme roughness that contributes to its hydrophobic properties.[49] The commercial applications of AKD surfaces are relatively limited due to its waxy physical properties and the fact that it must be applied with a certain minimum thickness to allow formation of the fractal surface. Furthermore, its resistance to rubbing is limited.

The transformation from smooth melt form to rough fractal form is both a time- and temperature-dependant pro-

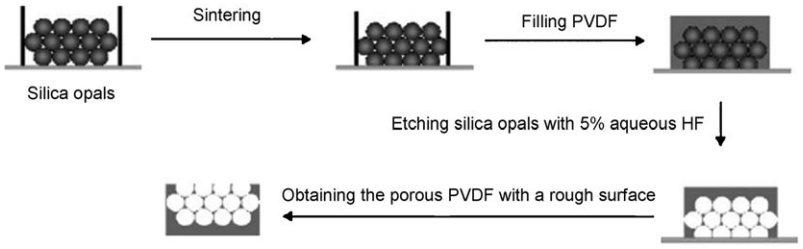

Figure 16. Schematic for the construction of PTFE microporous surfaces. The surfaces are altered by using different sized silica opals and changing the sintering temperatures. Reproduced with permission from ref. [45].

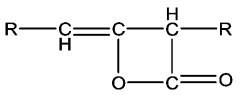

Figure 17. The chemical structure of an AKD (alkyl–ketene dimer) molecule in which R is a long alkyl chain (with chain length of around 16 carbon atoms). The alkyl chains will interact hydrophobically due to their non-polar nature, whereas the polarised C–O bonds can interact in a hydrophilic manner.

cess.[50] The surface structure naturally develops as the AKD cures and the fractal structure becomes rougher with time. The temperature at which the surface is cured also affects its hydrophobicity. It takes a shorter time to move to its fractal structure at temperatures close to the melting point of AKD (66 °C), and thus develops hydrophobicity faster at higher temperatures.[50]

An example of AKD synthesis uses stearoyl chloride ($CH_3(CH_2)_{16}COCl$) and triethylamine (Figure 18).[49] The AKD was isolated from the reaction mixture, then melted and left to solidify on a glass plate. The formation of the fractal surface during solidification occurs in an unprompted process. The AKD is susceptible to hydrolysis to form a dialkylketone (DAK) impurity (Figure 18), and the amount of this impurity can be used to control the hydrophobicity of the surface.[48]

The surface constructed from a 98 % AKD melt gives a water contact angle of 174° (Figure 19). The water contact angle achieved on a flat non-fractal AKD surface prepared by mechanical cutting is 109°. This change in the water contact angle on going from a flat to a rough surface shows the major effect the extreme roughness has on the hydrophobic properties of this material.[49]

The addition of surfactants to AKD has also been investigated.[50] It has been shown that, regardless of polarity, the addition of any surfactant decreased the water contact angle from the maximum value measured for an unaltered surface. The decrease in hydrophobicity is due to the ionic component of the surfactant interacting with the water. However, it was shown that small additions of non-polar surfactants could improve the sliding of a water droplet with little reduction in contact angle.[50]

Poly(alkylpyrrole): Poly(alkylpyrrole) has much in common with AKD in that it also has the potential to form a fractal surface.[51] The difference is that poly(alkylpyrrole) requires an electrochemical synthesis that includes the application of a potential difference during the polymerisation reaction.

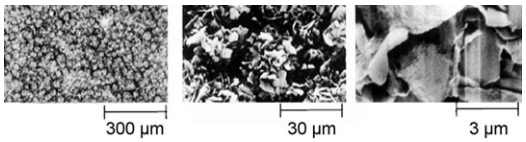

Figure 19. AKD surfaces at different magnifications (SEM images). Surfaces were left to solidify for 3 d under an inert N_2 atmosphere at RT. Reproduced with permission from ref. [49].

The result is a highly rough surface, which includes the formation of microtube structures formed without the need for a template.[51] The structure of the poly(alkylpyrrole) (Figure 20) indicates no particular water repellent component other than the alkyl R group.

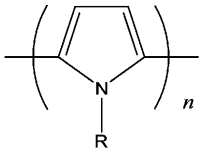

Poly(alkylpyrrole)

Figure 20. The structure of poly(alkylpyrrole), which has potential for the partial attraction of water through interactions with slightly polarised C–N bonds and the opportunity for electrophilic attraction with the aromatic system. It is, however, the high surface roughness that can be generated by this material that is the key to the super-hydrophobic properties.

One known construction of poly(alkylpyrrole) uses 1-*n*-octadecylpyrrole that is polymerised by the addition of sodium *p*-toluenesulfate (Figure 21).[52] The reaction is carried out under an applied voltage, which results in a build-up of polymer on the plate electrode over 1 h (in comparison, AKD surfaces need ≈3 d to form the fractal pattern). A water contact angle of 154° was achieved.

The coating exhibited no change in contact angle when treated with organic solvents or oils, due to a particularly high chemical stability and a stable geometric structure (Figure 22).

Chemically altered metal surfaces: Unaltered metal surfaces do not usually display hydrophobic characteristics.[53] Most metals can be shaped mechanically and the surface structure

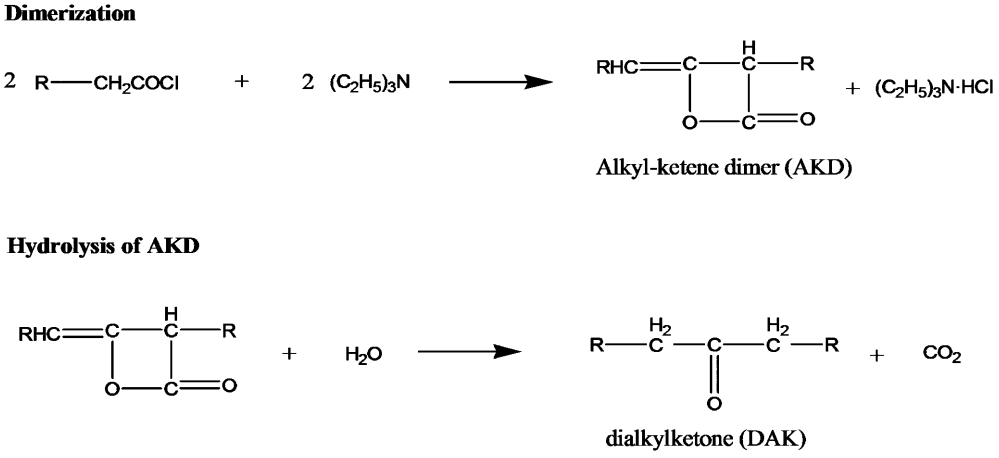

Figure 18. The dimerisation reaction gives the AKD after loss of hydrochloric acid. AKDs react with water to form the dialkylketone with loss of carbon dioxide. R = alkyl group ($(CH_2)_{15}CH_3$). Reproduced with permission from ref. [49].

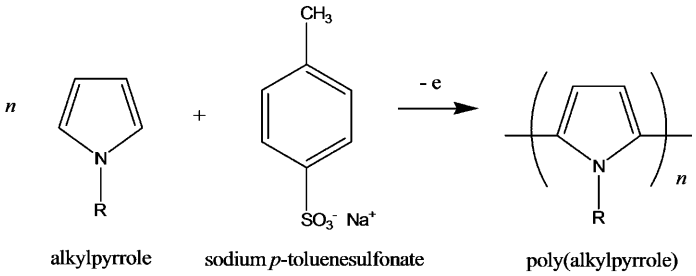

Figure 21. The reaction of 1-*n*-octadecylpyrrole (alkylpyrrole) with sodium *p*-toluenesulfate, under an applied potential difference, to give the poly(alkylpyrrole); $R = (CH_2)_{17}CH_3$.

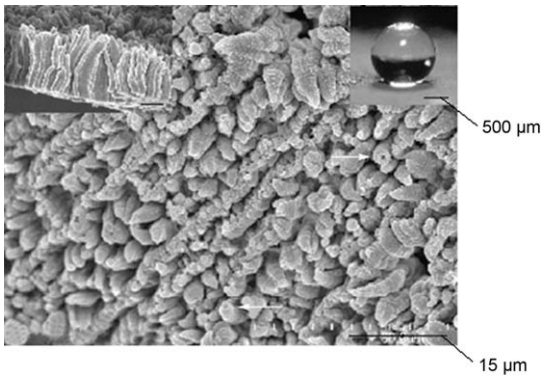

Figure 22. SEM image of the surface microstructure for the poly(alkylpyrrole). Inset: A view of a water droplet on the super-hydrophobic surface. Reproduced with permission from ref. [52].

becomes super-hydrophobic. It is the methyl groups on the PDMS that provide a surface with a low energy.[55] When applied to a rough surface, the hydrophobic nature of the PDMS is magnified, which allows for a super-hydrophobic surface with a water contact angle of 158°. Plain roughened copper had a contact angle of 23°, therefore, it is the application of the PDMS that makes it hydrophobic. The surface is stable over a range of pH values (1–14) and furthermore, water contact angles over these pH values were all hydrophobic.

The use of electrodeposition techniques has been utilised to grow wire-like surfaces on copper substrates.[56] Mumm et al.[56] deposited copper nanowires that were thermally oxidised to form a copper oxide layer, which renders them hydrophobic. This surface resulted in a very high water contact angle of 171°. Electrodeposition onto copper has also been used on pre-roughened copper (by etching); in this case electrodeposition of fluorinated polymers was carried out to give super-hydrophobic surfaces.[57] Further reactions of copper include the spray-coating of various substrates with copper alkylcarboxylates. These long-chain molecules act to lower the energy of the surface, and the spray-coating process helps to achieve a high surface roughness.[58]

Platinum nanowires have been formed by electrodeposition onto a Ti/Si substrate by using H_2PtCl_6 as a platinum source using anodic aluminium oxide (AAO) as a porous template.[59] The result is a network of nanowires that form a highly rough surface structure. The nanowires themselves are hydrophilic, with contact angles below 90°, so coating is designed with a great deal of accuracy, but because of the inherent hydrophilic nature of metals, roughening typically brings about enhanced hydrophilicity.[9] Therefore, metals must be chemically altered before they can be used in the design of hydrophobic surfaces. This is normally achieved by roughening the metal and then coating the surface with a hydrophobic material.

The modification of copper as a substrate has been performed.[54] This process involved pre-treatment of the copper with an aqueous solution of $K_2S_2O_8$ and KOH that oxidises the surface to form a thin layer of copper oxide. The resultant surface morphology is highly rough (Figure 23) and when coated in a hydrophobic material, such as polydimethylsiloxane (PDMS), the surface

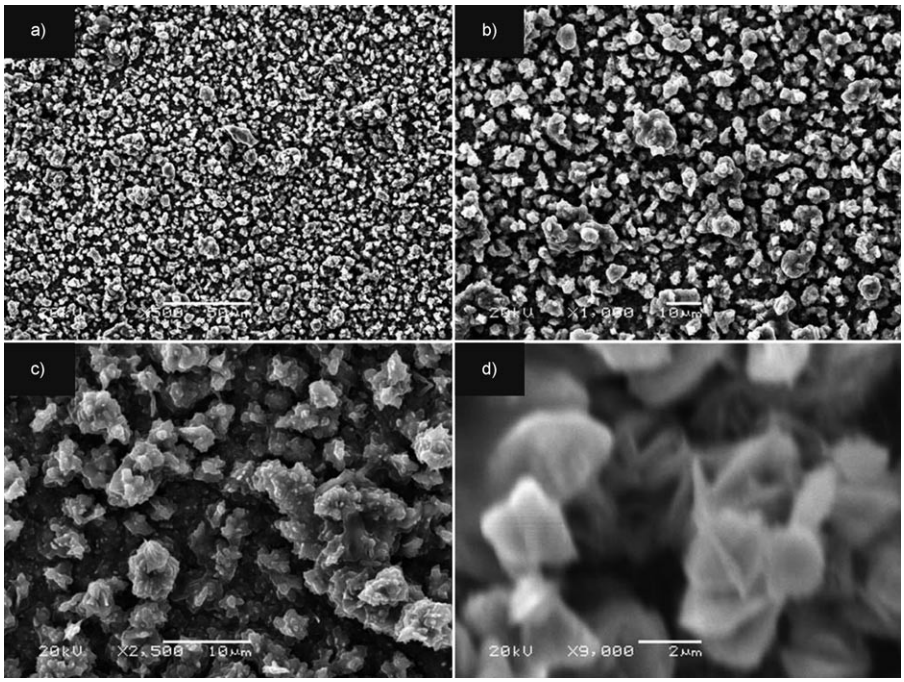

Figure 23. SEM images of an oxidised copper surface before the application of PDMS at various magnifications. The high surface roughness of the uncoated surface gives rise to water contact angles of 23°, but when the surface is coated with PDMS water contact angles around 158° are observed. Scale bars: a) 50 µm, b) 10 µm, c) 10 µm, d) 2 µm. Reproduced with permission from ref. [54].

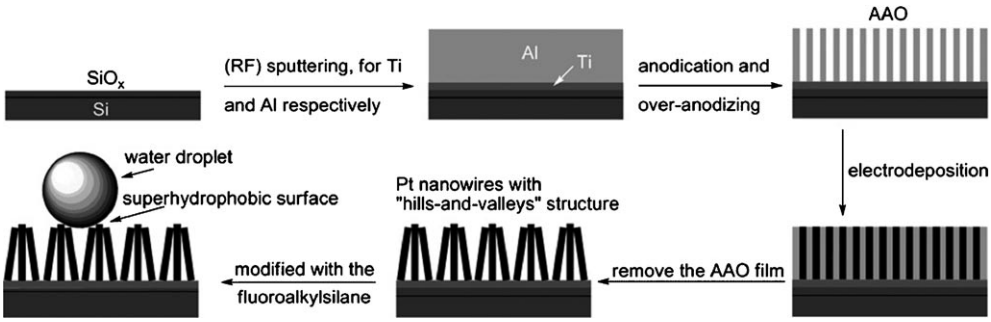

Figure 24. Schematic showing the method for generating Pt nanowires on a Ti/Si substrate, this surface is rendered super-hydrophobic by coating it with FAS molecules to give water contact angles of 158°. Reproduced with permission from ref. [59].

required to lower the surface energy. The nanowires were modified by the addition of a FAS molecule (CF_3-$(CF_2)_7CH_2CH_2Si(OCH_3)_3$), which provides a low surface energy and thus hydrophobicity. The combination of high surface roughness with the low-energy FAS gives a contact angle of 158° (Figure 24).[59]

A similar surface has been prepared by using ZnO nanowires.[60] The ZnO nanowires were grown hydrothermally in solution by using ZnO nanocrystals embedded in a cotton substrate as points for growth. The nanowires were then coated with a monolayer of FAS molecules to increase the hydrophobicity of the surface. The surface roughness combined with the hydrophobicity of the FAS monolayer gave a water contact angle of 161°.[60] FAS molecules can be used to modify other nanorods in a similar way.[61]

Copper mesh has been oxidised by using a solution of NaOH and $K_2S_2O_8$, to form $Cu(OH)_2$ nanoneedles upon oxidation. The needles are 7 μm in length, 150 to 300 nm in diameter and spread evenly over the mesh (Figure 25). When treated with a solution of *n*-dodecanethiol ($H_3C(CH_2)_{11}SH$), the surface converts to nanoneedles of $Cu(SC_{12}H_{25})_2$. The modification lowers the surface energy by adding C–H bonds that, when combined with the intrinsic surface roughness, generate a surface with a water contact angle of 151°.[62] This super-hydrophobic copper mesh can be used to separate solvents from water (Figure 26, top). 1:1 mixtures of water and solvent (solvent = hexane, petroleum ether, toluene and diesel oil) could be separated with at least 97% efficiency. By tuning the tilt angle, droplet rolling length and mesh pore size, the separation can be optimised to >99% separation efficiency.[62] Miniature boats have been constructed from a similar super-hydrophobic mesh made with *n*-dodecanoic acid instead of a thiol (Figure 26, bottom). Pore sizes of up to 930 μm were constructed, with buoyancy increasing with smaller pore size.[63]

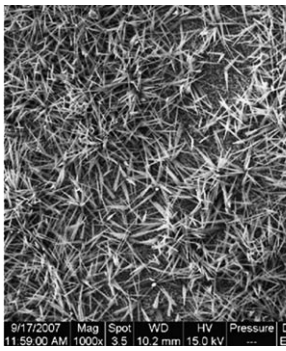

Figure 25. SEM image of the uniform coverage of $Cu(OH)_2$ nanoneedles on the surface before modification with *n*-dodecanethiol. The increased surface roughness of the copper mesh combined with the low energy provided by the C–H bonds of the thiol gives a water contact angle of 151°. Reproduced with permission from ref. [62].

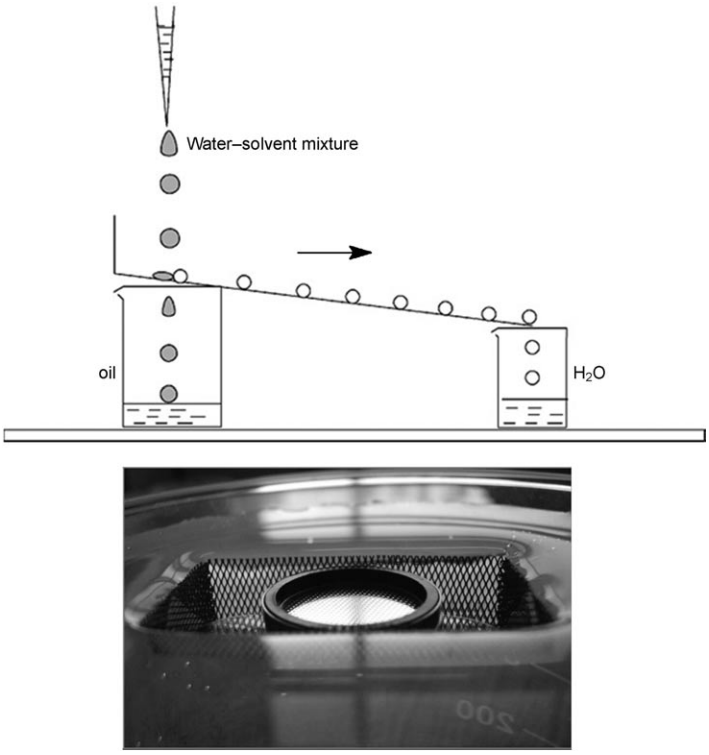

Figure 26. Top: Water–solvent mixtures added at a rate of 1 drop per second onto a super-hydrophobic copper mesh allows the water to fall on to the mesh and roll into a separate vessel, whereas the solvent freely permeates the mesh and falls through without travelling down the tilted copper. Bottom: A weighted miniature boat (dimensions: 4×2×1 cm) constructed from super-hydrophobic copper mesh floats on water. Reproduced with permission from ref. [62].

Iron–platinum nanoparticles have also been used as a way of roughening surfaces. The nanoparticles were prepared by using platinum acetylacetonate and $[Fe(CO)_5]$ in the presence of both long-chain carboxylic acids and thiols. The surface-bound ligating groups can then be exchanged for hydrophobic molecules through substitution reactions (Figure 27). The particles were spread onto a silicon substrate and the solvent was allowed to evaporate. The resultant surface structure is quite rough and, combined with the low energy of the fluorinated thiol and carboxylic acids, allowed for water contact angles of 160° to be obtained.[64] The use of long-chain molecules is a well-defined method for lowering surface energy.[65] An example of this is a synthesis that involves the application of a long-chain carboxylic acid to Co_3O_4 nanoscale powders that have been modified by using steric acid, giving a surface with a water contact angle of 155°.[66]

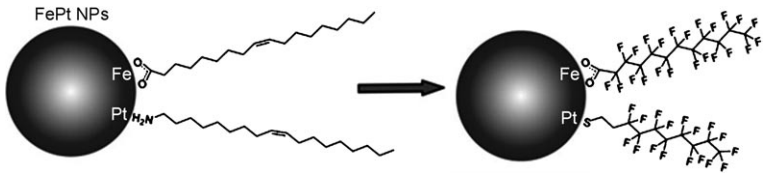

Figure 27. A ligand substitution reaction increases the hydrophobicity of the nanoparticles. Reproduced with permission from ref. [64].

Carbon nanotubes: Carbon nanotubes[67] can be grown in a variety of ways, which gives rise to many structures[68] (Figure 28). The rod-shaped structures can be arranged to provide a high surface roughness,[69] which is achieved by arranging the carbon nanotubes into "nanoforests". The hydrophobicity of unmodified, vertically aligned nanotubes is such that water contact angles of around 126° are obtained. However, carbon nanotubes can compress and collapse on interacting with water;[70,71] this results in a reduction in the contact angle the water makes with the surface. Methods have been developed for constructing resilient carbon nanotube "forests", and combining this with a surface modification with hydrophobic molecules can provide super-hydrophobic surfaces.[69]

To overcome carbon nanotube deformation, multi-walled carbon nanotubes (MWCNTs) can be used to stick the tubes to the substrate with an amorphous carbon deposition.[69] The adherent MWCNTs have a potentially higher resistance to stress and strain, thus deformation upon interaction with solvent is reduced. The nanotubes can be coated with nitrene molecules that introduce side groups in a UV-initiated process (Figure 29). The fluoroalkyl

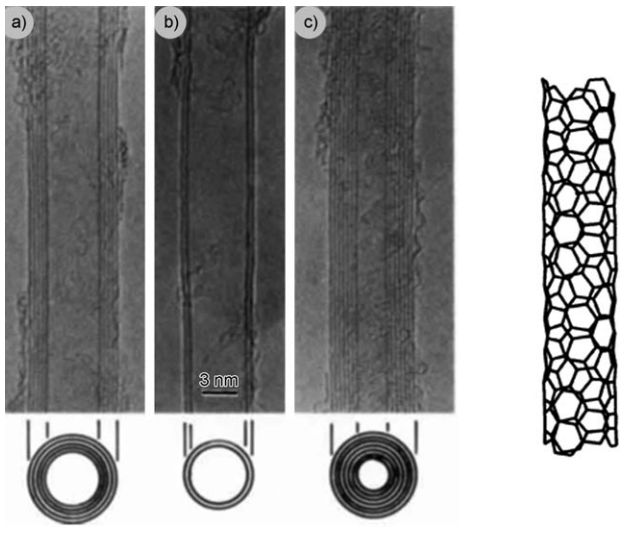

Figure 28. Left: SEM images of carbon nanotubes with a) five-, b) two- and c) seven-sheet nanotubes. Right: The arrangement of carbon atoms in one type of carbon nanotube. Reproduced with permission from refs. [67,72].

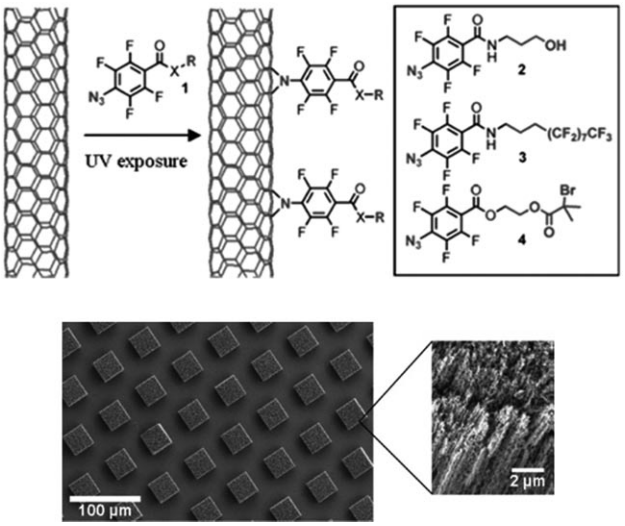

Figure 29. Top: Attachment of functionalised nitrenes to MWCNTs changes the wetting nature of the surface. Bottom: Patterned surface structure consisting of vertically aligned nanotubes attached to a surface. Reproduced with permission from ref. [69].

nitrene (**3**) was used to form a super-hydrophobic surface with a water contact angle of 161°. In comparison, the hydrophilic hydroxyalkyl nitrene coating (**2**) gives a water contact angle of close to 0°. By tuning the side chain, the properties of the surface can be altered, with its hydrophobicity/hydrophilicity being magnified by the high surface roughness of the carbon nanotube.

MWCNTs have also been used to pattern surfaces.[73] A Si substrate was spin-coated with a photoresist, then exposed to UV light to remove the photoresist and develop the sur-

face pattern. Electron-beam evaporation was then used to form a layer of Al/Fe catalyst (10 nm Al, 2 nm Fe), to be used for the carbon nanotube deposition, over the entire surface. Removing the photoresist with acetone developed the pattern shown in Figure 30. MWCNTs were then grown on the catalyst in a water-assisted thermal chemical vapour deposition process at 750–800 °C.

The patterning of the surface slightly increased the water contact angle achieved from 163° to 165°; however, the angle at which water droplets began to slide on the surface was significantly altered. The un-patterned MWCNT surface could hold a 2 μL water droplet at a 90° tilt and even upside-down (180°). Comparing this with the patterned surface, which had an average sliding angle of around 8°, it can be seen that the two surfaces wet in a very different way. The low sliding angle for the patterned surface suggests a Cassie–Baxter type wetting mechanism (see above), whereas the sticky nature of the un-patterned surface suggests a Wenzel mechanism. This is probably due to the voids in the pattern allowing air to be trapped underneath the water droplets and thus making it easier for the water to move across the surface. Silica microspheres have been used a substrate to bring an inherent roughness to the surface that would be hard to achieve with just carbon nanotubes.[74] Plasma action on aligned carbon nanotubes has also been carried out to render the tips of the nanotubes amorphous and increase the surface hydrophobicity.[75]

Modified silica-based surfaces: The surface of silica has many surface hydroxyl (silanol) groups; water droplets making contact with the surface will interact with these polar groups through hydrogen bonding and thus the surface of silica is hydrophilic.[76] To decrease the interaction of water with these groups, the surface can be heated and the hydroxyl groups removed[76] or the surface groups can be functionalised.[77] A silica surface can be rendered hydrophobic by lowering the surface energy or by attaching groups to the hydroxyl groups that do not interact with water (Figure 31). To improve the surface hydrophobicity through this method, surface roughness must be introduced. Superhydrophobic modification of surface silanol groups is commonly done by using FAS molecules,[78–81] in which this functionalisation is combined with roughening.

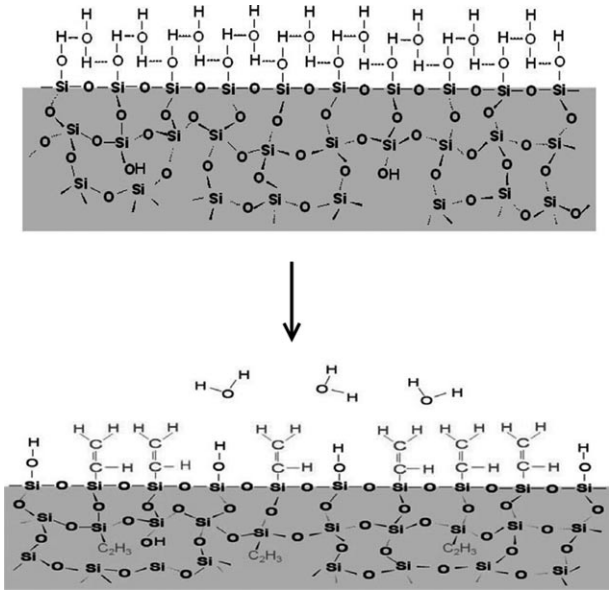

Figure 31. Schematic diagram showing the functionalisation of the surface hydroxyl groups on silica. Treatment of a flat silica substrate with these groups lowers the surface energy and makes the surface hydrophobic. Reproduced with permission from ref. [77].

Fumed silica is made up of nanoparticulate silica with diameters around 10 nm. It is formed by pyrolysis of $SiCl_4$ in the presence of oxygen and hydrogen. The particles agglomerate together, with more agglomeration occurring at higher temperatures. The small size means that there is a large surface area to mass ratio ($>100\ m^2\ g^{-1}$), which can be tuned to dictate the amount of agglomeration.[82] The relatively large surface area of fumed silica gives rise to potential functionalisation. By using a sol–gel process, silica nanoparticles were partially embedded in an organosilane network

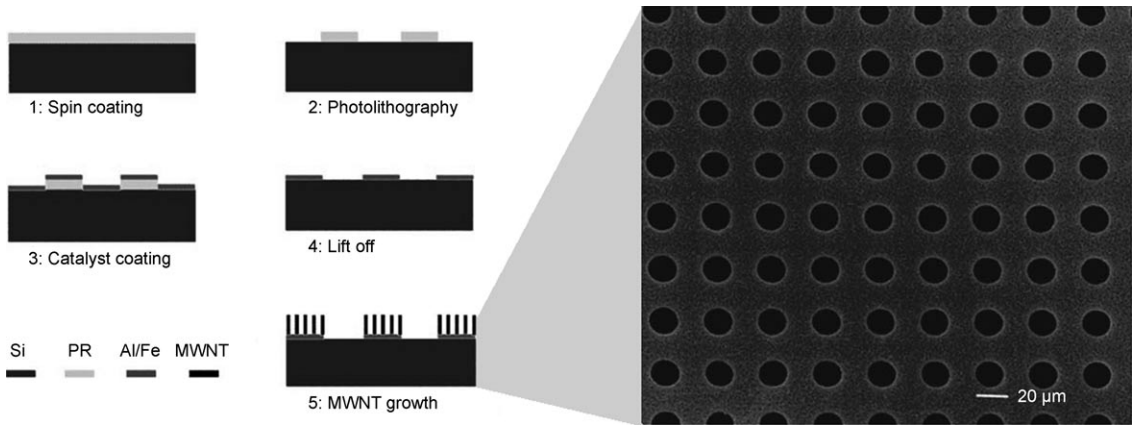

Figure 30. Left: Summary of the process used to generate the patterned surface and the growth of the MWCNTs. Right: An SEM of the patterned, nanotube coated surface. Reproduced with permission from ref. [73].

through spin-coating onto glass.[83] The fumed silica was functionalised by using hexamethyldisilazane to give surface groups of trimethylsiloxane (Figure 32). The rough and functionalised silica surfaces were super-hydrophobic, with a maximum water contact angle of 168° and tilt angles of less than 3°. The hydrophobicity of the films was reduced by outdoor exposure because the top layers of the fumed silica were removed. The rate of degradation of the films could be slowed by varying the relative amount of hexamethyldisilazane in the sol processing. The silica films were transparent, providing a high optical transmittance of around 92% and thus providing potential for self-cleaning window coatings.

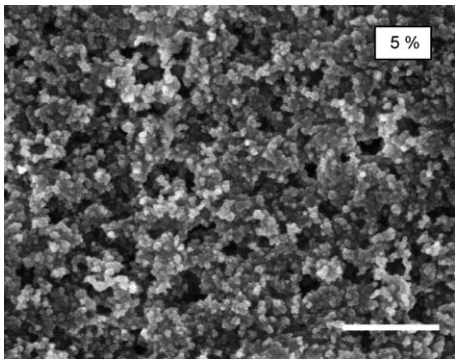

Figure 32. SEM image showing the film obtained by spin-coating a solution of 5 wt% trimethylsiloxane and silica nanoparticles in methyl isobutyl ketone onto glass. The fumed silica particles are approximately 10 nm in diameter and the agglomeration and embedding of these particles gives rise to the high surface roughness. The functionalisation with surface trimethylsiloxane groups lowers the surface energy (scale bar 200 nm). Reproduced with permission from ref. [83].

The use of silica nanoparticles as a method of surface roughening can provide a solid structure with low surface energy.[84] The coating can be made either by replacing the surface silanol groups on the nanoparticles[85,86] or by simply forming a thin layer of hydrophobic material.[87] This method of surface formation can be carried out at low temperatures, which means that surfaces such as cotton fibres can be coated and thus rendered super-hydrophobic.[88] A variation of this method uses colloidal zinc hydroxide with functionalisation of the surface hydroxyl groups by using bulky stearate groups. The modified zinc particles were then embedded in a silica network by spray-coating with a silica sol. The result is a super-hydrophobic surface, stated as achieving a water contact angle of 165°.[89]

The acid hydrolysis of tetraethylorthosilicate (TEOS) has been used in the formation of silica films.[90] Hydrolysis of silica followed by mixing with polypropylene glycol (PPG) to cast a film has been carried out. Pyrolysis of these films results in decomposition of the PPG and results in surface roughening. Changing the amount of PPG in the network gives a different degree of roughening. Modification of the surfaces was carried out by a reaction with HMDS that resulted in surface tetramethylsilane (TMS) groups that lowered the surface energy (Figure 33). Water contact angles of around 160° were recorded on the roughest surfaces, but these surfaces lacked high optical transparency (less than 30%). However, the transmittance could be improved by changing the pH of the reaction mixture and the ratio of TEOS to PPG. An optical transparency of greater than 97% was observed on a surface with water contact angle of 156°. Silica formation by using TEOS as a precursor has also been implemented as a support for silicon carbide nanowires, which also allows for super-hydrophobic surfaces.[91]

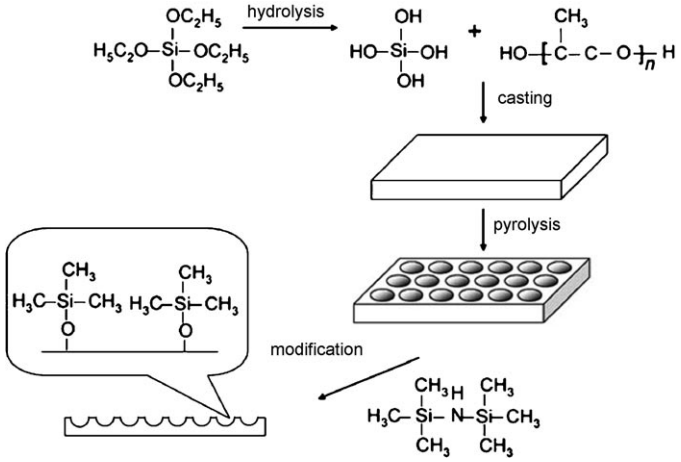

Figure 33. Schematic for the preparation of roughened silica films, followed by surface functionalisation with TMS groups. Reproduced with permission from ref. [90].

Chemical vapour deposition (CVD) of hydrophobic surfaces: The deposition of hydrophobic films by using CVD is currently an area of great interest.[32] The CVD process involves a gas-phase reaction of molecules inside a reactor followed by deposition onto substrates, which means that a wide range of possibilities can be explored. This section gives examples of some of the most successful methods for forming super-hydrophobic coatings.

Carbon nanotubes (CNTs): The CVD deposition of CNTs[92,93] results in a highly rough structure that allows for potentially very hydrophobic surfaces. Because the CNTs are by nature slightly hydrophilic, water contact angles on un-altered CNTs can be around 70 to 80°.[94] However, their high surface roughness means they have the ability to form very hydrophobic surfaces if modified with a low surface energy. Compounds such as CF_4 can be used in the CVD process to allow fluorination of the CNTs, this fluorination results in an increase in hydrophobicity. Water contact angles as large as 165° have been recorded on fluorinated CNTs formed by CVD.[95]

Polytetrafluoroethylene (PTFE): This coating can provide a very low energy surface, and has been used to CVD coat

rough surfaces to form extremely hydrophobic materials. Plasma-enhanced CVD (PECVD) uses plasma energy that can act to activate the precursors and/or change surface structure.[96] PECVD can be used to deposit films of PTFE-type materials to give water contact angles of $>100°$ on flat substrates; if a roughened microstructure is introduced to increase the surface roughness this improves to over 160°.[97]

Recent developments have demonstrated that surface roughness can be introduced during the PECVD process.[98] By pulsing the plasma energy through the fluorocarbon source (in this case hexafluorobenzene, C_6F_6), small particles are generated and agglomerate to form large features that are big enough to create a highly rough surface (Figure 34)

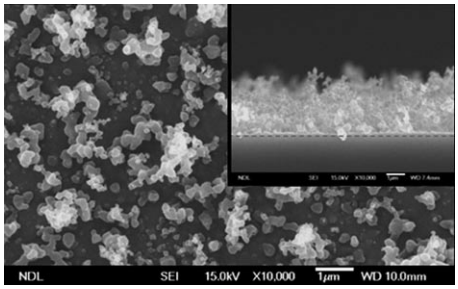

Figure 34. SEM of a super-hydrophobic surface constructed by using pulsed PECVD. Pulses of plasma are required for the agglomeration of the material into a film (scale bars 1 μm). Reproduced with permission from ref. [98].

on which water contact angles of over 160° can be achieved.[98] Solid PTFE can also be used as a precursor in a PECVD process. Gupta et al.[99] used electron pulses fired at PTFE discs to create PTFE vapours that were deposited onto silicon substrates, this achieved water contact angles of 166°.

Other examples of PECVD include use of a methylsilane (trimethylmethoxysilane, $(CH_3)_3Si(OCH_3)$) to form hydrophobic surfaces.[100] The additional use of microwave energy was used to activate the plasma further (MPECVD). Breakdown of trimethylmethoxysilane resulted in the presence of Si–CH_x, Si–H, Si–CH_2–Si, and Si–O–CH_3 groups on the surface, as well as a highly developed rough surface microstructure. The water contact angle for these siloxane surfaces was over 150°.[100] Another precursor used to construct a similar surface is hexamethylcyclotrisiloxane. Upon plasma activation of this molecule, chains and rings of methylated siloxanes were formed.[101] The result was a superhydrophobic surface with water contact angle of 162°.

Aerosol deposition: The use of PDMS-type materials has enabled hydrophobic surfaces to form through the coating of rough surfaces. There are commercially available curable silicone elastomers (e.g., Sylgard 184) that form PDMS-type structure from liquid precursors.[102] Crick et al. carried out the aerosol-assisted chemical vapour deposition (AACVD) of a solution of Sylgard 184 in which the balls of solvent in the aerosol were passed into a CVD reactor and heated. Upon evaporation of the solvent, the heat-curable silicone elastomer solidified and was deposited on to glass substrates. This one-step process formed a highly rough film made up of PDMS material (Figure 35). The water contact angle rose from 95° on a flat, dip-coated surface to 167° on the aerosol CVD film.[103]

Atmospheric pressure deposition: The deposition of WSe_2, formed by reacting tungsten hexachloride and diethyl selenide, onto an SiO_2-coated glass surface was carried out.[104] A water contact angle of 145° was achieved (Figure 36), and the surface structures were found to be made up of thin needles oriented predominantly perpendicular to the plane of the substrate. The high roughness of the film facilitated the maximisation of the water contact angle. However, the films exhibit Wenzel-type wetting, with no air trapped beneath the droplet. This resulted in droplets that did not roll or slide even at high tipping angles; this is due to a high surface–droplet contact area. Water droplets of up to 100 mg were stationary at a 90° tip angle. This unusual wetting be-

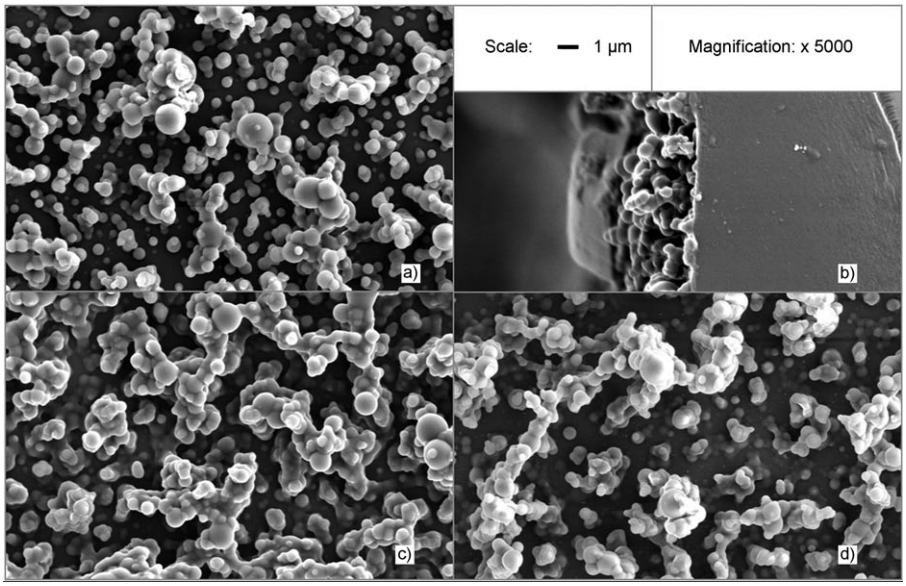

Figure 35. SEM images of Sylgard 184 silicone elastomer applied to glass substrates by using AACVD. The diagram shows the change in surface structure with deposition temperatures of a,b) 270, c) 300 and d) 360 °C. a,c,d) Top-down views of the films, b) profile view.

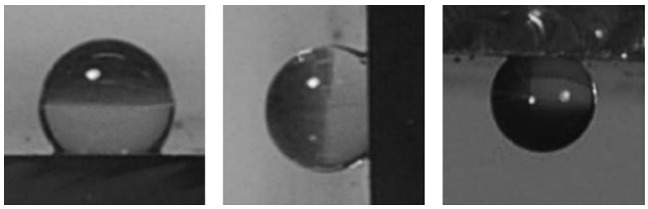

Figure 36. Shows water droplets sitting on a tungsten–selenide film tipped to angles of 0° (left), 90° (centre) and even suspended upside down (right). This clearly demonstrates the effect of the wetting nature on the interaction between water and a surface. Reproduced with permission from ref. [104].

haviour was, however, not demonstrated by similar diselenide systems ($TiSe_2$,[105] VSe_2,[106] $NbSe_2$,[107] $MoSe_2$[108]).

The formation of poly-*p*-xylylenes is a contrasting example of a Cassie–Baxter wetting surface. This surface was formed by the evaporation of aromatic and fluorinated precursors that resulted in a gas-phase reaction to form a poly-*p*-xylylene surface with a water contact angle of 153°.[109]

Miscellaneous surfaces

Lithographic imprinting: Lithographic imprinting involves moulding a natural lotus leaf surface (Figure 37). The imprinting was made by pouring a PDMS pre-polymer onto a

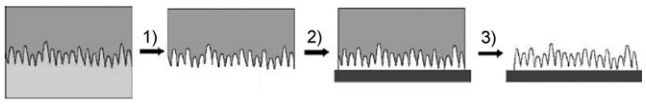

Figure 37. The process of imprinting: 1) A PDMS stamp is prepared by placing it on the surface of the leaf; 2) the stamp is pressed onto the ink (for only a few seconds); 3) the stamp is peeled off and dried to give an inverse lotus leaf-type surface. Reproduced with permission from ref. [110].

lotus leaf, which was used as a cast. After curing, the pre-polymer was separated from the leaf to give a negative of the lotus leaf structure. This imprinting of the pre-polymer was used to mould a BP-AZ-CA ink (see Figure 38) into a lotus leaf-type structure, which was then dried in vacuum. The resultant surface gave a water contact angle of 154.6°.[110] The BP-AZ-CA ink used is a long-chain polymer (Figure 38), the structure of which is not completely made up of water-repelling components (i.e., alkyl or fluoroalkyl chains); therefore, it is the high roughness of the lotus-like surface that contributes mostly to its super-hydrophobicity. The ink molecule must be polar to some degree for it to set

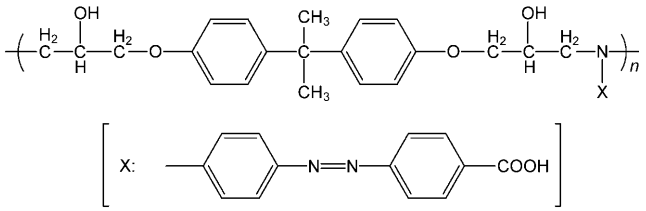

Figure 38. The [BP-AZ-CA] ink molecule used to form the hydrophobic surface. This is moulded into shape by pressing the PDMS pre-polymer stamp into the "lotus leaf" structure. The hydrophilic parts of the molecule include the carboxyl and hydroxyl groups, but their hydrophilicity is reduced by their close proximity to the aromatic systems.

in the moulded form when stamped by the PDMS imprinting.

Low-density polyethylene has also been used to cast the lotus leaf,[111] which resulted in a replication of the microstructure of the lotus leaf by using a low-energy material. The replicated surface was capable of achieving a 154° water contact angle. A similar example uses polystyrene in the casting of a honeycomb structure. The top layer of the honeycomb is then peeled away to leave the spike that once connected the top and bottom layers. The spiked low-energy surface was reported to achieve a water contact angle of 165°.[112]

PDMS is a low-energy material that can be roughened to form a super-hydrophobic surfaces.[113] However, PDMS has also been used as a substrate onto which a mono-layer of close-packed silica spheres was transferred (Figure 39).[114] The silica spheres were coated in silver nanoparticles by interaction with $[Ag(NH_3)_2]^+$ ions, then chemically modified with perfluorodecanethiol (PFT) to lower the surface energy. The combination of the roughness brought about by the spheres and the lowered surface energy allowed for water contact angles of 156° to be achieved. The PDMS substrates are flexible and have some transparency, so this rubber-like super-hydrophobic material could be applied to other materials.

Electro-spinning of polystyrene (nanoporous surfaces): The silver ragwort leaf was a source of inspiration for one generated structure[115] that exhibits highly rough nanostructures. The aim was to form such a structure on the same nanometre scale through electro-spinning.[116–118] Electro-spinning involves the application of a voltage to polystyrene solutions as they are being deposited on a collector. In this example,[115] the polystyrene solutions were made with varying compositions of tetrahydrofuran (THF) and *N*,*N*-dimethylformamide (DMF). The surface structures made this way

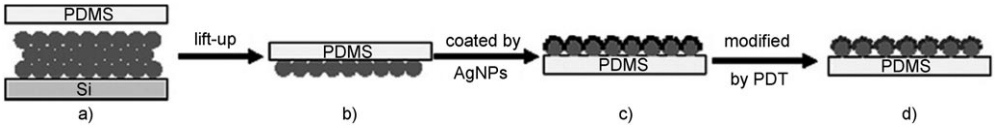

Figure 39. Schematic of the soft lithography of silica spheres followed by functionalisation with silver nanoparticles and then perfluorodecanethiol (PDT). Reproduced with permission from ref. [114].

were quite porous, with the most hydrophobic surface resulting from a THF/DMF ratio of 1:3, which gave a highly rough and porous surface (Figure 40). This mixture gave a water contact angle of 159.5°.

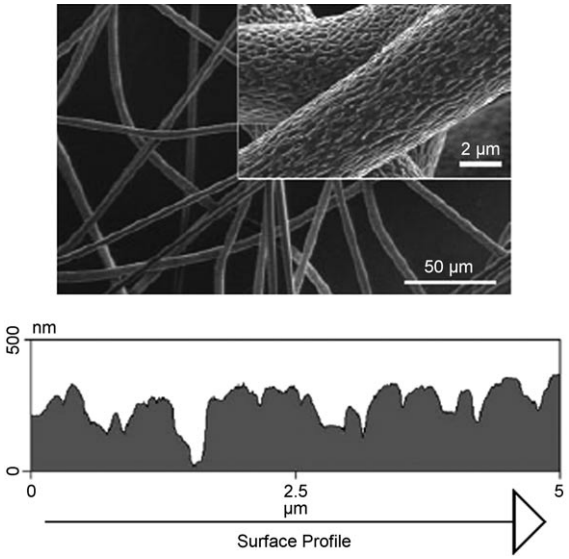

Figure 40. Top: SEM image of the electro-spun polystyrene surface and bottom: an atomic force microscopy (AFM) cross-sectional surface profile. Both images are of a surface formed with a THF/DMF ratio of 1:3, which results in the most hydrophobic surface. Reproduced with permission from ref. [115].

The key to controlling the hydrophobicity of the surface was the solvent ratio used, with ratio of 1:3 of THF/DMF giving an optimal surface (see above). This results in air being trapped beneath any water droplets on the surface, which reduces the amount of liquid–surface contact and thus the surface is rendered super-hydrophobic. The microstructure (Figure 40) can be seen to resemble that of the silver ragwort leaf.[115] The electro-spinning of poly(vinylidene fluoride) is an alternative precursor.[119] The energy of the resultant surface was lowered by the addition of an FAS compound, which has also been used in other electro-spinning experiments.[120] This method can be applied to many compounds.[116–118]

Routes and Applications of Hydrophobic Surfaces

Routes to hydrophobicity: The techniques discussed in this review have led to the development of four main routes for construction of hydrophobic surfaces. In the design of superhydrophobic surfaces, there are two main features that must be focussed on: a low surface energy so a flat surface has a contact angle above 90° and a high surface roughness to amplify the hydrophobicity of the surface. The surface roughness can be introduced when depositing the low-energy material[98] or it can be introduced separately,[38] which results in either a one-step construction (laying down a rough low-energy surface) or a two-step construction (introducing surface roughness then lowering the surface energy), see Figure 41. Surface roughness can also be introduced to a low-energy material, such as PTFE,[38] and used as-is, or roughening can be performed on a low-energy material applied to a substrate by the application of AKD.[121]

The routes have different issues to consider. Route **1a** requires the use of low-energy material that has good adherence to the substrate. If it has no adherence, the film will be powdery and will be of limited use. Route **1b** only requires the use of a low-energy material that can be roughened and has the ability to survive the roughening process. The two-step formation, **2a**, needs the material used for roughening to have some affinity for the hydrophobic reagent. If there is no adherence, the hydrophobic coating will be of limited use because it will easily separate from the surface features. A variation of the two-step technique involves the roughening of an already low-energy surface (**2b**), this requires that the low energy of the material is maintained upon roughening, and that adherence to the original substrate is also maintained. If the low-energy material is not maintained, the introduced roughness will not be benefited from.

Applications of hydrophobic surfaces: Hydrophobic surfaces have many applications in a wide number of fields. Methods for fabrication have been described in the previous section, here we will focus on the range of employment of such surfaces.

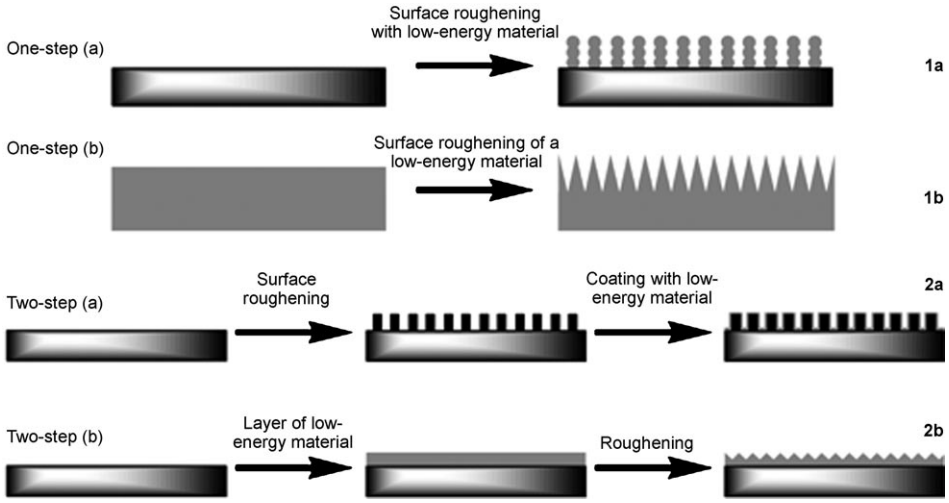

Figure 41. Schematic showing the four main mechanisms (**1a**, **1b**, **2a**, **2b**) for the construction of a hydrophobic surface.

Lotus effect self-cleaning coatings (anti-biofouling): It has been demonstrated that surface coatings can be designed for the removal of particles upon treatment with water by duplicating the lotus effect. Figure 42 shows one plain Formica sheet and one coated with PTFE that have both been dusted with soot particles. Upon spraying with water, the particles were completely removed from the PTFE-treated sheet. The untreated sheet did not demonstrate the lotus effect and thus did not self-clean on exposure to water. A paint that dries to form a hydrophobic surface and possesses significant self-cleaning attributes has also been introduced into the marketplace (Sto AG).[122] Suppression of bacterial adhesion to a surface has also been a key goal for self-cleaning surfaces; it has been shown that super-hydrophobic surfaces can be used not only to clear a surface of dirt particles and bacteria, but also to severely limit bacterial adhesion and growth.[123]

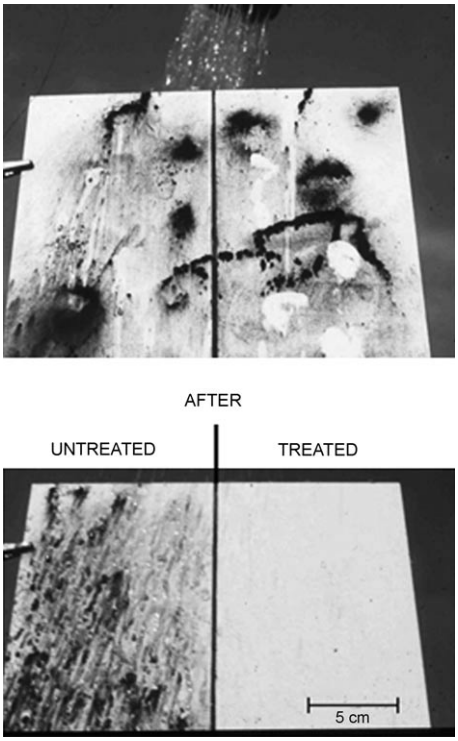

Figure 42. Soot-coated Formica plates. The left plate in each image is an untreated surface that shows no lotus-effect self-cleaning thus soot removal is inefficient. The right plate in each image is coated with micropowdered PTFE to give a super-hydrophobic surface from which soot is easily removed with water. Reproduced with permission from ref. [122].

There is also a substantial area of research focussed toward transparent super-hydrophobic self-cleaning coatings. Transparent films applied to see-through glasses and plastics could be utilised in industries such as automotives, buildings and solar panels. This would insure that transparency is maintained due to the self-cleaning of the surface.[124] Super-hydrophobic coatings such as the lotus leaf require a rough microstructure. To generate a transparent coating, the features of the surfaces roughness must have dimensions less than the wavelength of visible light ($\lambda \approx 380$–760 nm).[125] Given this, the surface microstructure formation must be carefully considered if transparency is one of the desired properties.

Despite these factors, there is a wide range of products on the market that are aimed toward transparent hydrophobic applications.[126–128] Hydrophobic surfaces can prevent adhesion of bacteria to surfaces,[123] for example, a commercially available spray for ship hulls limits biofouling by reducing the ability of bacteria to stick to the surface.[129] Applications for windows (domestic and vehicular) are also available;[126,130] these coatings act to keep the glass free of sticking water droplets and also to produce a window with self-cleaning properties, so that water droplets carry away dirt and bacteria. With respect to car windscreens, products aim to make the glass slippery[131,132] to allow the fast removal of water. Spectacle glass is also an area of commercial exploitation for hydrophobic coatings.[133]

Surface protection: A super-hydrophobic surface limits the contact between water and a surface, therefore, if a metal surface was rendered super-hydrophobic then corrosion would be limited. Experiments carried out on copper, in which surface oxidation followed by functionalisation gave rise to super-hydrophobic copper surfaces, promise corrosion prevention.[134] This technology could be applied to other forms of surface protection from water. Hydrophobic surfaces not only repel water droplets but show resistance to humidity. Fluorinated silanes have been used to coat paper to give a super-hydrophobic surface that rendered the paper resistant to humidity, that is, its tensile strength was maintained up to very high humidity.[135]

Textiles: Textiles such as cotton already have some surface roughness, so treatments to render them super-hydrophobic can be performed. Treatments of paper[135] and cotton fabric[136,137] have been carried out to make super-hydrophobic materials. Changing the textiles from their natural hydrophilic form to being extremely water repellent means that not only will the fabric be kept dry, but the flexibility and insulating properties can be maintained. Figure 43 shows cotton fibres that have been coated by using a sol–gel method. Nanosized silver was also incorporated into the coating to give antimicrobial activity to the cotton. The roughness brought about by the fibres used in textile design means that water-repellent fibre can be used and the inherent roughness of fabrics (Figure 43) can help magnify the surface hydrophobicity. The development of hydrophobic textiles is known and there are many commercially available products.[138,139]

Movement of water: The Cassie–Baxter model suggests a slippery surface that allows water to move across it with ease, whereas a Wenzel-type surface would be more resistant to water movement. This is because the resistance to

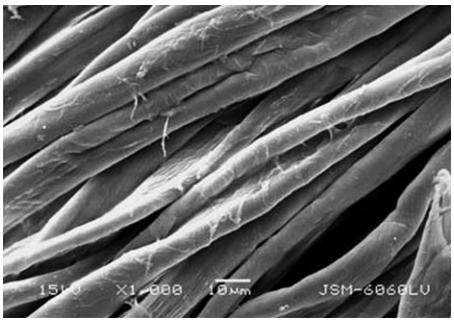

Figure 43. SEM image of super-hydrophobic cotton fabric coated with a fluoroalkyl siloxane. The fibres allow for an initial surface roughness that then can be coated with a low-energy material (scale bar 10 μm). Reproduced with permission from ref. [137].

drag is reduced on a Cassie–Baxter-type surface due to the layer of gas at the liquid–solid interface. Experiments in which the insides of copper pipes are coated so that they are super-hydrophobic show that there is significant reduction in water drag through them (see Figure 44 for the experimental setup).[140] The super-hydrophobic tube allows a greater rate of flow through when put under the same pressure of water. Also, commercially available treatments for boat hulls can reduce drag in the water and allow the craft to travel more easily through the water,[129] and the area of drag reduction has also been academically researched.[141] Another effect of the layer of gas at the water–solid interface stems from the buoyancy of water. Objects with a Cassie–Baxter wetting mechanism will have a volume of air between the surface and the water when floating on a body of water. This volume of air acts with a buoyancy supporting force.[142]

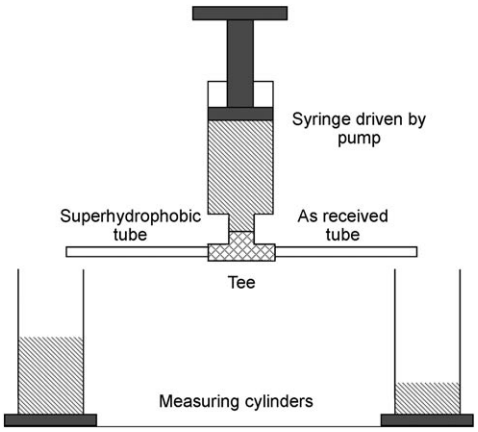

Figure 44. Experimental setup to demonstrate the faster movement of water through super-hydrophobic tubing relative to unaltered tubing. The faster movement is due to the decreased drag force between the water and the walls of the super-hydrophobic tubes. Reproduced with permission from ref. [140].

The repulsion of water from a super-hydrophobic surface also has the effect of limiting contact of any components in the water with the surface. This can be important in areas such as artificial organ implantation, in which the adhesion of platelets to blood-containing vessels can cause coagulation or thrombosis.[143]

Microfluidics: Another application of hydrophobic surfaces is in the movement of water on a microscale. It has been shown that by altering the wetting properties of a surface, the ability of water to move on it can be controlled,[144] and it is possible to manipulate water droplets by controlling the surface microstructure.[145] Water movement at the microscale is important in areas such as biofluid transport,[146] in which wetting behaviour and, therefore, water movement can be controlled by changes in voltage or temperature.[144]

Oil–water separation: Using water-repellent molecules, such as long alkyl chains, to coat a surface and lower its energy could not only result in the surface becoming super-hydrophobic but could also give superoleophilic properties.[62] Copper mesh modified to be super-hydrophobic and then tilted will let water roll off, but substances such as hexane, petroleum ether, toluene and diesel oil are not repelled like the water and are allowed to slip through the mesh. Mixtures of water and oily substances can thus be separated with up to and above 99% efficiency. Super-hydrophobic nanoporous polymers have been investigated and have been found to be very effective absorbers of organic compounds.[147] These materials could act to absorb any oil-like products and leave water behind, and may be able to be implemented in the cleanup of oil spillages at sea.

Summary and Outlook

This review shows that a wide range of methods for forming super-hydrophobic surfaces are available, and the chosen method strongly depends on the potential applications of the surface. For example, transparent coatings must have surface features that do not interact with light.[125] The wetting mechanism of the surface must also be considered; if self-cleaning is desired, for example, then Cassie–Baxter wetting must take place. Some of the examples used in this review do not try to cover the slip angle of water on the surface, which leaves a gap in the understanding of the surface interaction with water. To allow super-hydrophobic surfaces to be directly compared and contrasted through the literature, similar methods for analysis must be used (e.g., contact angles). The classification of surface construction methods into types **1a**, **1b**, **2a** and **2b** allows an understanding of the design necessary for the formation of super-hydrophobic surfaces.

Acknowledgements

I.P.P. and C.R.C. thank the EPSRC for funding. Prof. David Sheel is thanked for discussions on related projects. I.P.P. thanks the Royal Society/Wolfson Trust for a merit award.

[1] X. Zhang, F. Shi, J. Niu, Y. Jiang, Z. Wang, *J. Mater. Chem.* **2008**, *18*, 621.
[2] X. Li, D. Reinhoudt, M. Crego-Calama, *Chem. Soc. Rev.* **2007**, *36*, 1350.
[3] G. McHale, N. J. Shirtcliffe, M. I. Newton, *Langmuir* **2004**, *20*, 10146.
[4] M. Ma, R. M. Hill, *Curr. Opin. Colloid Interface Sci.* **2006**, *11*, 193.
[5] W. Att, N. Hori, F. Iwasa, M. Yamada, T. Ueno, T. Ogawa, *Biomaterials* **2009**, *30*, 4268.
[6] Z. Cui, L. Yin, Q. Wanga, J. Ding, Q. Chen, *J. Colloid Interface Sci.* **2009**, *337*, 531.
[7] W. Barthlott, C. Neinhuis, *Planta* **1997**, *202*, 1.
[8] Y. Cheng, D. E. Rodak, *Appl. Phys. Lett.* **2005**, *86*, 144101.
[9] Z. Burton, B. Bhushan, *Ultramicroscopy* **2006**, *106*, 709.
[10] C. Neinhuis, W. Barthlott, *Ann. Bot.* **1997**, *79*, 667.
[11] X. Gao, L. Jiang, *Nature* **2004**, *432*, 36.
[12] M. Sun, G. S. Watson, Y. Zheng, J. A. Watson, A. Liang, *J. Exp. Biol.* **2009**, *212*, 3148.
[13] Y. Zheng, X. Gao, L. Jiang, *Soft Matter* **2007**, *3*, 178.
[14] S. Lee, T. H. Kwon, *Nanotechnology* **2006**, *17*, 3189.
[15] R. N. Wenzel, *Ind. Eng. Chem.* **1936**, *28*, 988.
[16] A. B. D. Cassie, S. Baxter, *Trans. Faraday Soc.* **1944**, *40*, 546.
[17] V. Rico, P. Romero, J. L. Hueso, J. P. Espinós, A. R. González-Elipe, *Catal. Today* **2009**, *143*, 347.
[18] A. B. D. Cassie, *Discuss. Faraday Soc.* **1948**, *3*, 11.
[19] J. Kim, H. Sugimura, O. Takai, *Vacuum* **2002**, *66*, 379.
[20] A. Marmur, *Langmuir* **2003**, *19*, 8343.
[21] N. A. Patankar, *Langmuir* **2003**, *19*, 1249.
[22] P. Roach, N. J. Shirtcliffe, M. I. Newton, *Soft Matter* **2008**, *4*, 224.
[23] A. M. Peters, C. Pirat, M. Sbragaglia, B. M. Borkent, M. Wessling, D. Lohse, R. G. H. Lammertink, *Eur. Phys. J. E* **2009**, *29*, 391.
[24] S. M. Lee, C. Y. Park, S. Bae, J. S. Go, B. Shin, J. S. Ko, *Jpn. J. Appl. Phys.* **2009**, *48*, 095504.
[25] J. Liu, X. Feng, G. Wang, S. Yu, *J. Phys. Condens. Matter* **2007**, *19*, 356002.
[26] W. Choi, A. Tuteja, J. M. Mabry, R. E. Cohen, G. H. McKinley, *J. Colloid Interface Sci.* **2009**, *339*, 208.
[27] S. A. Kulinich, M. Farzaneh, *Appl. Surface Sci.* **2009**, *255*, 4056.
[28] F. Chang, S. Hong, Y. Sheng, H. Tsao, *Appl. Phys. Lett.* **2009**, *95*, 064102.
[29] S. Wang, L. Jiang, *Adv. Mater.* **2007**, *19*, 3423.
[30] G. J. Toes, K. W. van Muiswinkel, W. van Oeveren, A. J. H. Suurmeijer, W. Timens, I. Stokroos, J. J. A. M. van den Dungen, *Biomaterials* **2002**, *23*, 255.
[31] A. M. Almanza-Workman, S. Raghavan, S. Petrovic, B. Gogoi, P. Deymier, D. J. Monk, R. Roop, *Thin Solid Films* **2003**, *423*, 77.
[32] E. L. Decker, S. Garoff, *Langmuir* **1997**, *13*, 6321.
[33] K. Koch, B Bhushan, Y. C. Jung, W. Barthlott, *Soft Matter* **2009**, *5*, 1386.
[34] D. Brutin, Z. Zhu, O. Rahli, J. Xie, Q. Liu, L. Tadrist, *Microgravity Sci. Technol.* **2009**, 21, 67.
[35] W. Wu, X. Wang, X. Liu, F. Zhou, *Appl. Mater. Interfaces* **2009**, *1*, 1656.
[36] Y. Akamatsu, K. Makita, H. Inaba, T. Minami, *Thin Solid Films* **2001**, *389*, 138.
[37] M. Mostefaï, Y. Auriac, M. E. R. Shanahan, J. Bressan, A. Meslif, *Int. J. Adhes. Adhes.* **2000**, *20*, 257.
[38] J. Bico, C. Marzolin, D. Quere, *Europhys. Lett.* **1999**, *47*, 220.
[39] A. Nakajima, K. Abe, K. Hashimoto, T. Watanabe, *Thin Solid Films* **2000**, *376*, 140.
[40] J. Lu, Y. Yu, J. Zhou, L. Song, X. Hub, A. Larbot, *Appl. Surface Sci.* **2009**, *255*, 9092.
[41] S. R. Coulson, I. Woodward, J. P. S. Badyal, S. A. Brewer, C. Willis, *J. Phys. Chem. A* **2000**, *104*, 8836.
[42] E. Bormashenko, V. Goldshtein, R. Barayev, T. Stein, G. Whyman, R. Pogreb, Z. Barkay, D. Aurbach, *Polym. Adv. Technol.* **2009**, *20*, 650.
[43] A. Milella, R. Di Mundo, F. Palumbo, P. Favia, F. Fracassi, R. d′Agostino, *Plasma Processes Polym.* **2009**, *6*, 460.
[44] W. Song, D. D. Veiga, C. A. Custódio, J. F. Mano, *Adv. Mater.* **2009**, *21*, 1830.
[45] J. Li, J. Fu, Y. Cong, Y. Wu, L. Xue, Y. Han, *Appl. Surface Sci.* **2006**, *252*, 2229.
[46] J. Yang, Z. Zhang, X. Men, X. Xu, *J. Macromol. Sci. Part A* **2009**, *46*, 997.
[47] I. S. Bayer, A. Steele, P. J. Martorana, E. Loth, L. Miller, *Appl. Phys. Lett.* **2009**, *94*, 163902.
[48] L. Yan, K. Wang, L. Ye, *J. Mater. Sci. Lett.* **2003**, *22*, 1713.
[49] S. Shibuichi, T. Onda, N. Satoh, K. Tsujii, *J. Phys. Chem.* **1996**, *100*, 19512.
[50] R. Mohammadi, J. Wassink, A. Amirfazli, *Langmuir* **2004**, *20*, 9657.
[51] H. Yan, H. Shiga, E. Ito, T. Nakagaki, S. Takagi, T. Ueda, K. Tsujii, *Colloids Surf.* **2006**, *284*, 490.
[52] H. Yan, K. Kurogi, H. Mayama, K. Tsujii, *Angew. Chem.* **2005**, *117*, 3519; *Angew. Chem. Int. Ed.* **2005**, *44*, 3453.
[53] R. Wang, L. Cong, M. Kido, *Appl. Surface Sci.* **2002**, *191*, 74.
[54] Z. Guo, W. Liu, B. Su, *Appl. Phys. Lett.* **2008**, *92*, 063104.
[55] M. Jin, X. Feng, J. Xi, J. Zhai, K. Cho, L. Feng, L. Jiang, *Macromol. Rapid Commun.* **2005**, *26*, 1805.
[56] F. Mumm, A. T. J. van Helvoort, P. Sikorski, *ACS Nano* **2009**, *3*, 2647.
[57] Z. Kang, Q. Ye, J. Sang, Y. Li, *J. Mater. Process. Technol.* **2009**, *209*, 4543.
[58] W. Wu, X. Wang, X. Liu, F. Zhou, *Appl. Mater. Interfaces* **2009**, *1*, 1656.
[59] M. Qu, G. Zhao, Q. Wang, X. Cao, J. Zhang, *Nanotechnology* **2008**, *19*, 055707.
[60] B. Xu, Z. Cai, *Appl. Surface Sci.* **2008**, *254*, 5899.
[61] D. Tian, Q. Chen, F. Nie, J. Xu, Y. Song, L. Jiang, *Adv. Mater.* **2009**, *21*, 3744.
[62] Q. Pan, M. Wang, H. Wang, *Appl. Surface Sci.* **2008**, *254*, 6002.
[63] Q. Pan, M. Wang, *Appl. Mater. Interfaces* **2009**, *1*, 420.
[64] Y. Ofir, B. Samanta, P. Arumugam, V. M. Rotello, *Adv. Mater.* **2007**, *19*, 4075.
[65] F. Zhang, L. Zhao, H. Chen, S. Xu, D. G. Evans, X. Duan, *Angew. Chem.* **2008**, *120*, 2500; *Angew. Chem. Int. Ed.* **2008**, *47*, 2466.
[66] Z. Yuan, H. Chen, C. Li, L. Huang, X. Fu, D. Zhao, J. Tang, *Appl Surface Sci* **2009**, *255*, 9493.
[67] S. Iijima, *Nature* **1991**, *354*, 56.
[68] M. Paradise, T. Goswami, *Mater. Des.* **2007**, *28*, 1477.
[69] S. J. Pastine, D. Okawa, B. Kessler, M. Rolandi, M. Llorente, A. Zettl, J. M. J. Fréchet, *J. Am. Chem. Soc.* **2008**, *130*, 4238.
[70] C. T. Wirth, S. Hofmann, J. Robertson, *Diamond Relat. Mater.* **2008**, *17*, 1518.
[71] J. S. Lee, J. Ryu, C. B. Park, *Soft Matter* **2009**, *5*, 2717.
[72] M. S. Dresselhaus, G. Dresselhaus, J. C. Charlier, E. Hernandez, *Philos. Trans. R. Soc. A* **2004**, *362*, 2065.
[73] Z. Wang, N. Koratkara, L. Ci, P. M. Ajayan, *Appl. Phys. Lett.* **2007**, *90*, 143117.
[74] L. Zhang, D. E. Resasco, *Langmuir* **2009**, *25*, 4792.
[75] M. Shakerzadeh, H. E. Teo, C. Tan, B. K. Tay, *Diamond Relat. Mater.* **2009**, *18*, 1235.
[76] J. Laskowski, J. A. Kitchener, *J. Colloid Interface Sci.* **1969**, *29*, 670.
[77] Q. Wei, Y. Wang, Z. Nie, C. Yu, Q. Li, J. Zou, C. Li, *Microporous Mesoporous Mater.* **2008**, *111*, 97.
[78] X. Liu, J. He, *Langmuir* **2009**, *25*, 11822.
[79] Q. F. Xu, J. N. Wang, I. H. Smith, K. D. Sanderson, *J. Mater. Chem.* **2009**, *19*, 655.
[80] T. Saison, C. Peroz, V. Chauveau, S. Berthier, E. Sondergard, H. Arribart, *Bioinspiration Biomimetics* **2008**, *3*, 046004.

[81] Q. F. Xua, J. N. Wang, *New J. Chem.* **2009**, *33*, 734.
[82] N. Auner, J. Weis, *Organosilicon Chemistry II: From Molecules to Materials*, Wiley, New York, **1996**, p. 761.
[83] M. Manca, A. Cannavale, L. De Marco, A. S. Aricò, R. Cingolani, G. Gigli, *Langmuir* **2009**, *25*, 6357.
[84] C. Liao, C. Wang, H. Lin, H. Chou, F. Chang, *Langmuir* **2009**, *25*, 3359.
[85] P. N. Manoudis, A. Tsakalof, I. Karapanagiotis, I. Zuburtikudis, C. Panayiotou, *Surf. Coat. Technol.* **2009**, *203*, 1322.
[86] Z. Qian, Z. Zhang, L. Song, H. Liu, *J. Mater. Chem.* **2009**, *19*, 1297.
[87] Z. Cui, L. Yin, Q. Wanga, J. Ding, Q. Chen, *J. Colloid Interface Sci.* **2009**, *337*, 531.
[88] G. Y. Bae, B. G. Min, Y. G. Jeong, S. C. Lee, J. H. Jang, G. H. Koo, *J. Colloid Interface Sci.* **2009**, *337*, 170.
[89] R. V. Lakshmi, B. J. Basu, *J. Colloid Interface Sci.* **2009**, *339*, 454.
[90] Q. Wei, Y. Wang, Z. Nie, C. Yu, Q. Li, J. Zou, C. Li, *Microporous Mesoporous Mater.* **2008**, *111*, 97.
[91] J. J. Niu, J. N. Wang, *J. Phys. Chem. B* **2009**, *113*, 2909.
[92] S. A. Miller, V. Y. Young, C. R. Martin, *J. Am. Chem. Soc.* **2001**, *123*, 12335.
[93] T. Kyotani, L. Tsai, A. Tomita, *Chem. Mater.* **1995**, *7*, 1427.
[94] D. Mattia, M. P. Rossi, B. M. Kim, G. Korneva, H. H. Bau, Y. Gogotsi, *J. Phys. Chem. B* **2006**, *110*, 9850.
[95] Y. C. Hong, D. H. Shin, H. S. Uhm, *Surf. Coat. Technol.* **2007**, *201*, 5025.
[96] J. Wang, F. Liu, H. Chen, D. Chen, *Appl. Phys. Lett.* **2009**, *95*, 084104.
[97] D. J. Balazs, C. Hollenstein, H. J. Mathieu, *Plasma Processes Polym.* **2005**, *2*, 104.
[98] S. H. Yang, C. Liu, W. Hsu, H. Chen, *Surf. Coat. Technol.* **2009**, *203*, 1379.
[99] S. Gupta, A. C. Arjunan, S. Deshpande, S. Seal, D. Singh, R. K. Singh, *Thin Solid Films* **2009**, *517*, 4555.
[100] Y. Wu, M. Kouno, N. Saito, F. A. Nae, Y. Inoue, O. Takai, *Thin Solid Films* **2007**, *515*, 4203.
[101] M. C. Kim, C.-P. Klages, *Surf. Coat. Technol.* **2009**, *204*, 428.
[102] M. Khoo, C. Liu, *Sens. Actuators A* **2001**, *89*, 259.
[103] C. R. Crick, I. P. Parkin, *J. Mater. Chem.* **2009**, *19*, 1074.
[104] N. D. Boscher, C. J. Carmalt, I. P. Parkin, *J. Mater. Chem.* **2006**, *16*, 122.
[105] N. D. Boscher, C. J. Carmalt, I. P. Parkin, *Chem. Vap. Deposition* **2006**, *12*, 54.
[106] N. D. Boscher, C. S. Blackman, C. J. Carmalt, I. P. Parkin, A. G. Prieto, *Appl. Surface Sci.* **2007**, *253*, 6041.
[107] N. D. Boscher, C. J. Carmalt, I. P. Parkin, *Eur. J. Inorg. Chem.* **2006**, 1255.
[108] N. D. Boscher, C. J. Carmalt, R. G. Palgrave, J. J. Gil-Tomas, I. P. Parkin, *Chem. Vap. Deposition* **2006**, *12*, 692.
[109] Y. Elkasabi, H. Nandivada, H. Chen, S. Bhaskar, J. D′Arcy, L. Bondarenko, J. Lahann, *Chem. Vap. Deposition* **2009**, *15*, 142.
[110] B. Liu, Y. He, Y. Fan, X. Wang, *Macromol. Rapid Commun.* **2006**, *27*, 1859.
[111] J. Feng, M. Huang, X. Qian, *Macromol. Mater. Eng.* **2009**, *294*, 295.
[112] W. Ting, C. Chen, S. A. Dai, S. Suen, I. Yang, Y. Liu, F. M. C. Chenad, R. Jeng, *J. Mater. Chem.* **2009**, *19*, 4819.
[113] S. J. Hwang, D. J. Oh, P. Gu Jung, S. M. Lee, J. S. Go, J. Kim, K. Hwang, J. S. Ko, *J. Micromech. Microeng.* **2009**, *19*, 095010.
[114] T. Yao, C. Wang, Q. Lin, X. Li, X. Chen, J Wu, J. Zhang, K. Yu, B. Yang, *Nanotechnology* **2009**, *20*, 065304.
[115] Y. Miyauchi, B. Ding, S. Shiratori, *Nanotechnology* **2006**, *17*, 5151.
[116] D. Reneker, I. Chun, *Nanotechnology* **1996**, *7*, 216.
[117] D. Li, Y. N. Xia Y, *Nano. Lett.* **2004**, *4*, 933.
[118] H. Q. Liu, Y. L. Hsieh, *J. Polym. Sci. Part B* **2002**, *40*, 2119.
[119] Y. Chen, H. Kim, *Appl Surface Sci* **2009**, *255*, 7073.
[120] T. Ogawa, B. Ding, Y. Sone, S. Shiratori, *Nanotechnology* **2007**, *18*, 165607.
[121] T. Minami, H. Mayama, K. Tsujii, *J. Phys. Chem. B* **2008**, *112*, 14620.
[122] A. Solga, Z. Cerman, B. F. Striffler, M. Spaeth, W. Barthlott, *Bioinspiration Biomimemtics* **2007**, *2*, S126.
[123] D. P. Bakker, F. M. Huijs, J. de Vries, J. W. Klijnstra, H. J. Busscher, H. C. van der Mei, *Colloids Surf. B* **2003**, *32*, 179.
[124] J. Fresnais, J. P. Chapel, F. Poncin-Epaillard, *Surf. Coat. Technol.* **2006**, *200*, 5296.
[125] A. Nakajima, *J. Ceram. Soc. Jpn.* **2004**, *112*, 533.
[126] http://www.saint-gobain-sekurit.com/EN/?nav1=PR&id=360.
[127] http://www.opticalcoatings.com/processes/hydrophobic.html.
[128] http://www.diamonfusion.com/en/products/applications.aspx.
[129] http://www.auroramarine.com/aurora/catalog/01250/.
[130] http://www.nanoprotect.co.uk/nanofor-car.html.
[131] http://www.rainx.co.uk/.
[132] http://www.aquapel.com/.
[133] http://www.mayerandmayer.com/more_info.asp?current_id=84.
[134] X. H. Chen, G. B. Yang, L. H. Kong, D. Dong, L. G Yu, J. M. Chen, P. Y. Zhang, *Cryst. Growth Des.* **2009**, *9*, 2656.
[135] H. Yang, Y. Deng, *J. Colloid .Interface Sci.* **2008**, *325*, 588.
[136] S. C. Cho, Y. C. Hong, S. G. Cho, Y. Y. Ji, C. S. Han, H. S. Uhm, *Curr. Appl. Phys.* **2009**, *9*, 1223.
[137] B. Tomšič, B. Simončič, B. Orel, L. Černe, P. F. Tavčer, M. Zorko, I. Jerman, A. Vilčnik, J. Kovac, *J. Sol-Gel Sci. Technol.* **2008**, *47*, 44.
[138] http://www.velouk.com/.
[139] http://www.salclear.com/DWR.htm.
[140] N. J. Shirtcliffe, G. McHale, M. I. Newton, Y. Zhang, *App. Mater. Inter.* **2009**, *1*, 1316.
[141] Y. Zhou, M. Li, B. Su, Q. Lu, *J. Mater. Chem.* **2009**, *19*, 3301.
[142] M. S. Żbik, J. Du, R. A. Pushkarova, R. St. C. Smart, *J. Colloid Interface Sci.* **2009**, *336*, 616.
[143] T. Sun, H. Tan, D. Han, Q. Fu, L. Jiang, *Small* **2005**, *1*, 959.
[144] T. Saitoh, A. Sekino, M. Hiraide, *Anal. Chim. Acta* **2005**, *536*, 179.
[145] J. Yang, J. C. Chen, K. Huang, J. A. Yeh, *J. Microelectromech. Syst.* **2006**, *15*, 697.
[146] P. Bayiati, A. Tserepi, P. S. Petrou, K. Misiakos, S. E. Kakabakos, E. Gogolides, C. Cardinaud, *Microelectron. Eng.* **2007**, *84*, 1677.
[147] Y. Zhang, S. Wei, F. Liu, Y. Du, S. Liu, Y. Ji, T. Yokoi, T. Tatsumi, F. Xiao, *Nano Today* **2009**, *4*, 135.

Published online: March 5, 2010

